Bull. Chem. Soc. Jpn., 72, 2573—2590 (1999)

Accounts

Positive Feedback Mechanism, Autocatalysis Mechanism, and Dependence on Atomic-Level Surface Structures in Electrochemical Oscillations for H_2O_2 Reduction on Pt Electrodes

Yoshiharu Mukouyama, Shuji Nakanishi, and Yoshihiro Nakato*

Department of Chemistry, Graduate School of Engineering Science, Osaka University, Toyonaka, Osaka 560-8531

(Received August 2, 1999)

Electrochemical reduction of H_2O_2 on Pt electrodes shows a variety of oscillations, depending on the electrode potential, electrode illumination, the atomic-level flatness of the electrode surface, and the presence or absence of metal atoms and halogen atoms adsorbed to submonolayer amounts on the electrode surface. This is a unique feature of this oscillating system, helpful for deeper understanding of oscillation phenomena. In this article, the fundamental behavior and mechanism of oscillations, named oscillations A and B, for polycrystalline Pt electrodes are first described. A mathematical simulation for oscillation A shows clearly the presence of a positive feedback mechanism and an important role of adsorbed hydrogen atoms, called upd-H. The behavior of oscillation A, especially the oscillation period, is changed by electrode illumination, application of weak external potential pulses, and coupling with other oscillation systems. The oscillation period is also altered by adsorption of foreign metal atoms such as Cu, Ag, Au, and Ru on Pt to sub-monolayer amounts. New-type oscillations called oscillations C and D appear when small amounts of halide ions are added to the solution. The appearance of oscillations C and D is explained by assuming a catalytic effect of adsorbed halogen atoms and an autocatalytic effect of adsorbed OH group on the H_2O_2 reduction. Another new-type oscillation is observed when an atomically-flat single-crystal Pt(111) electrode is used. These results clearly show an important role of atomic-level structures of the electrode surface in electrochemical oscillations.

Chemical and electrochemical oscillations have attracted growing attention as a typical example of non-linear phenomena. Chemical reactions in oscillating systems proceed synchronically in an in-phase mode, sometimes showing beautiful spatiotemporal patterns such as growing vortexes. Thus the oscillatory systems can be regarded as an appearance of dynamic self-organizing ability of molecular systems. Detailed investigations will give new insights into understanding of dynamic and highly organized molecular systems including living bodies and their functions.

Though the most famous oscillatory reaction, called the Belousov–Zhabotinsky reaction, is observed in a homogeneous solution,[1,2] a large number of oscillatory reactions have rather been observed in heterogeneous systems such as electrochemical reactions and catalytic reactions on solid surfaces, as summarized in recent reviews.[3—5] Moreover, electrochemical oscillations have great advantages for mechanistic studies, in that the oscillations and their coupling can be easily detected by measuring the electrode potential and current and that the Gibbs energies of reactions, which play a crucial role in oscillatory systems, can be changed continuously by shifting the electrode potential.

Electrochemical oscillations have been reported for various reactions such as anodic metal dissolution,[6,7] cathodic metal deposition,[8] oxidation of hydrogen[9,10] and small organic compounds,[11,12] and reduction of hydrogen peroxide[13—19] and peroxodisulfate.[20] We have studied electrochemical oscillations for reduction of hydrogen peroxide (H_2O_2) on Pt electrodes. Only a few studies[17,19] were reported on the "H_2O_2–acid–Pt electrode" oscillation system, concerning "oscillation A" described below, before our work. We have found a variety of oscillations of different types, named oscillations A, B, C, D, and E, depending on the electrode potential, the atomic flatness of the electrode surface, and the presence or absence of foreign metal atoms and halogen atoms adsorbed to submonolayer amounts on the electrode surfaces.[21—30]

The "H_2O_2–acid–Pt electrode" oscillation system is of much interest in the following respects: (1) The Pt electrode is stable during oscillations, only acting as an electrocatalyst. (2) The oscillations are caused by some fundamental reactions such as hydrogen evolution, hydrogen adsorption, and H_2O_2 reduction, which have been relatively well studied. (3) A variety of oscillations of different types are observed,

as mentioned above. Their comparative studies under common experimental conditions must be helpful for a deeper understanding of oscillation phenomena.

In the present paper, we survey our recent studies on the electrochemical oscillations for H_2O_2 reduction on Pt electrodes. The purpose of this review is to show the general behavior and the main features of the electrochemical oscillations, such as positive feedback mechanism, autocatalytic mechanism, and strong surface-structure dependence. Besides this purpose, one can understand through this review that studies of electrochemical oscillations are effective not only for exploration of non-linear phenomena but also for clarification of mechanisms of electrochemical reactions themselves.

1. Oscillations Observed for Polycrystalline Pt Electrodes

1.1. Fundamental Behavior and Reaction Models for Oscillations A and B. Let us first describe the behavior of oscillations observed for polycrystalline Pt electrodes.[21—25] The electrochemical oscillations can be measured by a simple experimental setup such as that shown in Fig. 1. A Pt disc (or wire or plate) can be used as the working electrode, together with a Pt plate as the counter electrode and a saturated calomel electrode (SCE) or an Ag/AgCl electrode as the reference electrode. The electrode potential (U) or the current (I) is regulated with a commercial potentio-galvanostat and potential programmer. The measured current and electrode potential are either recorded with an X–Y recorder or stored digitally with a Mac ADIOS II/16 (GW Instruments) at 1 or 10 kHz. The working electrode is placed statically without any rotating system. The electrolyte is also in most cases kept static without any stirring system. The current (I) or current density (j) vs. potential (U) curves are not corrected for ohmic drops in the solution, unless otherwise noted.

Figure 2 shows j–U curves for a polycrystalline Pt-disc electrode in 0.3 M H_2SO_4 (M = mol dm^{-3}) containing H_2O_2 of various concentrations.[22] All the curves are measured under potential-controlled conditions. One can easily see how the j–U curve changes with the H_2O_2 concentration, or in other words, under what conditions electrochemical oscillations appear. Figure 2(a) is a j–U curve in an electrolyte (0.3 M H_2SO_4) not containing H_2O_2. This is included to indicate cathodic and anodic current peaks in a region of 0.00 to −0.25 V vs. SCE, which are attributable to the formation and disappearance of electrochemically adsorbed hydrogen atoms, called upd-H (under-potential deposited hydrogen),

$$Pt + H^+ + e^- \underset{k_{-1}}{\overset{k_1}{\rightleftharpoons}} Pt\text{–}H \text{ (upd-H)} \qquad (1)$$

where Pt represents a surface Pt site schematically. The upd-H plays an important role in the appearance of oscillation A, as described later. The observation of two peaks for both the cathodic and anodic currents is characteristic of polycrystalline Pt electrodes. It is reported that upd-H is stable, located at three- or four-fold symmetry sites of surface Pt lattices, and does not contribute to hydrogen evolution.[31,32] A cathodic current peak at about 0.45 V in Fig. 2(a) is due to

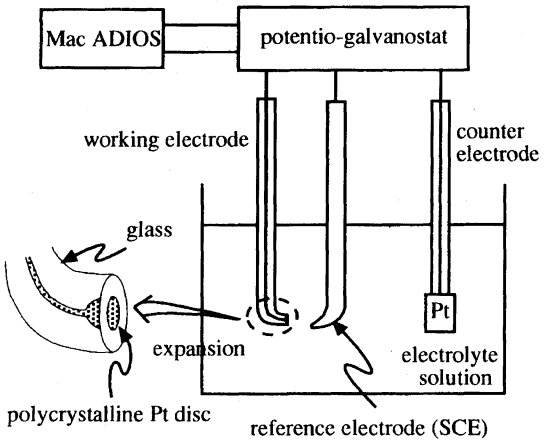

Fig. 1. Experimental setup for observing an electrochemical oscillation.

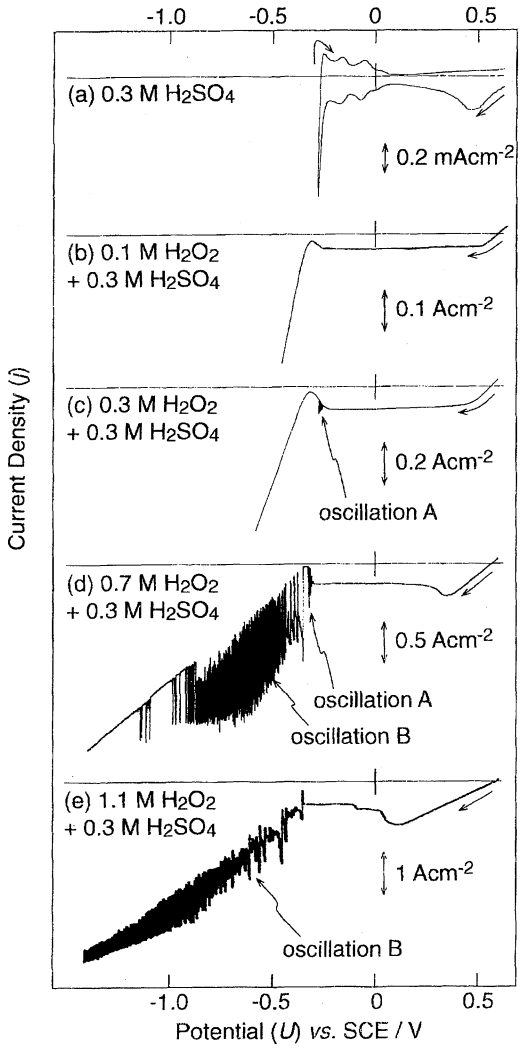

Fig. 2. Current density (j)–potential (U) curves for a polycrystalline Pt-wire (0.3 mm in diameter and 5 mm long) electrode in 0.30 M H_2SO_4 containing H_2O_2 in various concentrations, measured under a potential-controlled condition. The scan rate is 100 mV s^{-1}.

reduction of Pt oxide formed in more positive potentials.

When 0.1 M H_2O_2 is added to 0.3 M H_2SO_4 (Fig. 2(b)), a cathodic current due to H_2O_2 reduction appears. It starts at about 0.6 V vs. SCE and reaches the potential-independent current at around 0.4 V. (Note that the j scale in Figs. 2(b), 2(c), 2(d), and 2(e) is much larger than that in Fig. 2(a).) The following reactions can be assumed for the H_2O_2 reduction:

$$2Pt + H_2O_2 \xrightarrow{k_2} 2Pt\text{–}OH \quad (2)$$

$$Pt\text{–}OH + H^+ + e^- \xrightarrow{k_3} Pt + H_2O \quad (3)$$

Reaction (2) represents dissociative adsorption of H_2O_2 and can be regarded as a potential-independent process. Thus the observed potential-independent current in about 0.4 to -0.3 V in Fig. 2(b) can be explained by assuming that this process is a rate-determining step. At the initial stage of our work,[22,25] we assumed, according to the literature,[33–35] that the H_2O_2 reduction was initiated by reaction (2′),

$$Pt + H_2O_2 + H^+ + e^- \xrightarrow{k_{2'}} Pt\text{–}OH + H_2O \quad (2')$$

with the potential-independent current attributed to the diffusion limitation for H_2O_2. However, this model was denied experimentally,[30] as explained later.

In the above argument, we only considered the reduction of Pt–OH (or H_2O_2). However, the oxidation of Pt–OH

$$2Pt\text{–}OH \xrightarrow{k_4} 2Pt + O_2 + 2H^+ + 2e^- \quad (4)$$

will become important in positive potentials, i.e., near the onset potential of the H_2O_2-reduction current (ca. 0.6 V vs. SCE). A combination of reactions (2), (3), and (4) is equivalent to catalytic decomposition of H_2O_2 into O_2 and H_2O on Pt. In fact, gas bubbles are evolved at the electrode surface in potentials from about 0.6 to 0.4 V, indicating that the catalytic decomposition really occurs at the Pt surface.

The j–U curve in Fig. 2(b) shows a "negative slope" in a region from -0.25 to -0.33 V just before hydrogen evolution. A similar result was reported by Koper et al.[19] The "negative slope" is located at the most negative side of the two cathodic current peaks in Fig. 2(a), i.e., at the potential where the surface coverage of upd-H approaches its maximum. This implies that the H_2O_2 reduction, or reaction (2), is strongly suppressed by the formation of upd-H. The reason why upd-H suppresses reaction (2) is not clear at present because the formation of small upd-H at hollow Pt sites will exert almost no steric hindrance.

When the concentration of H_2O_2 is increased to 0.3 M (Fig. 2(c)), a current oscillation, called oscillation A, appears just in the potential region of the "negative slope".[17,19] This suggests that oscillation A is caused by suppression of the H_2O_2 reduction by formation of upd-H. Figures 3 and 4 show time-courses of oscillation A at various potentials and various H_2O_2 concentrations, respectively. Nearly rectangular-shaped oscillatory waves are observed. Figure 5 shows a reaction model for oscillation A on the basis of the above-

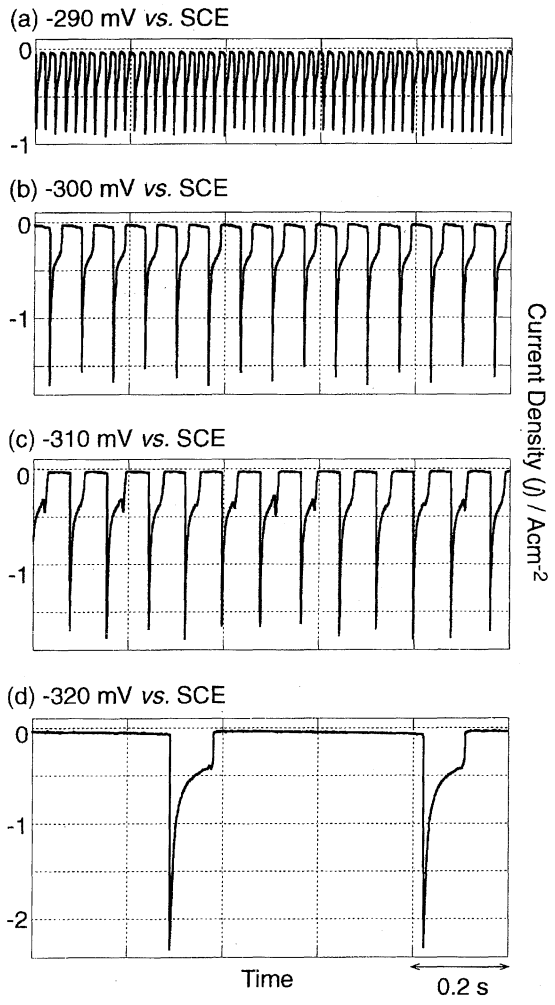

Fig. 3. The waveform of oscillation A as a function of the electrode potential (U). Electrode: a Pt disc of 1.0 mm in diameter. Electrolyte: 0.7 M H_2O_2+0.3 M H_2SO_4.

mentioned idea. The high-current (in the absolute value) state corresponds to active H_2O_2 reduction with no upd-H at the Pt surface, whereas the low-current state corresponds to strong suppression of the H_2O_2 reduction by formation of upd-H of a nearly full coverage. This model is supported by mathematical simulation, as explained later. It may be noted that the oscillation period increases with a negative shift of the potential (Fig. 3) and a decrease in the H_2O_2 concentration (Fig. 4).

When the concentration of H_2O_2 is made much higher to 0.7 M (Fig. 2(d)), another oscillation, called oscillation B, appears in a potential region of hydrogen evolution.[21,22] This implies that the appearance of oscillation B is closely related with hydrogen evolution on a Pt electrode. It is reported[31,32] that not upd-H but another type of adsorbed H, called "on-top H", contributes to hydrogen evolution by the following scheme.

$$Pt + H^+ + e^- \underset{k_{-5}}{\overset{k_5}{\rightleftharpoons}} Pt\text{–}H \text{ (on-top H)} \quad (5)$$

$$Pt\text{–}H \text{ (on-top H)} + Pt\text{–}H \text{ (on-top H)} \xrightarrow{k_6} H_2 \quad (6)$$

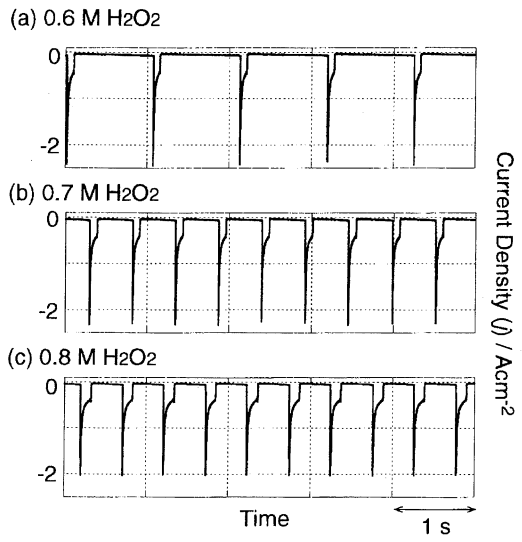

Fig. 4. The waveform of oscillation A as a function of the H_2O_2 concentration, with the H_2SO_4 concentration being kept 0.3 M. Electrode: a Pt disc of 1.0 mm in diameter. Electrode potential: −0.32 V vs. SCE.

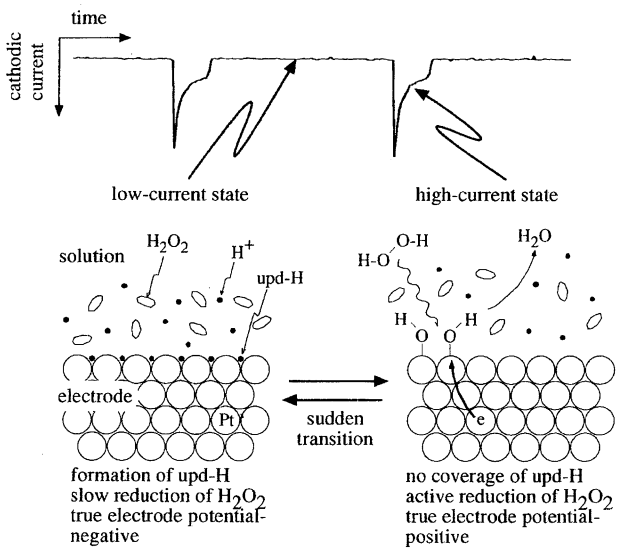

Fig. 5. Reaction model for the low- and high-current states of oscillation A.

However, mathematical simulation on the basis of these reactions cannot reproduce the appearance of oscillation B, as explained later.

Figure 6 shows a time course of oscillation B.[22] The oscillatory behavior of oscillation B is rather similar to that for oscillation A, though the wave pattern in Fig. 6 is somewhat modified by hydrogen-gas evolution at the electrode surface. It is to be noted that, for oscillation B, not only the current oscillation under a potential-controlled condition (Fig. 2(d)) but also the potential oscillation under a current-controlled condition are observed as shown in Fig. 7(b). On the contrary, no potential oscillation is observed for oscillation A. Figure 7(a) shows, for reference, a bistability characteristic observed under a current-controlled condition in a relatively low H_2O_2 concentration.

At a very high H_2O_2 concentration of 1.1 M, oscillation A disappears and only oscillation B is observed (Fig. 2(e)). At an even higher H_2O_2 concentration, both oscillations A and B disappear. Figure 8 shows a phase diagram for the appearance of oscillations A and B with respect to the H_2O_2 and H_2SO_4 concentrations.[25] We can see that not only the H_2O_2 and H_2SO_4 concentrations but also their ratios are important for the appearance of oscillations A and B.

1.2. Mathematical Simulation. For deeper understanding of the mechanisms of oscillations, it is important to reproduce them by mathematical simulation. The first mathematical model for electrochemical oscillations was proposed by Franck and FitzHugh[6] to explain current oscillations in anodic dissolution of iron electrodes in acid solutions. Recently, a simpler model was developed by Koper and Sluyters[36,37] for modelling oscillations involving metal deposition[36] and metal dissolution,[37] and later successfully applied to oscillating H_2O_2-reduction on p-$CuInSe_2$[38] and n-GaAs.[39] Oscillation A in the present work can be reproduced and analyzed on the basis of this model.[25]

We first consider an equivalent circuit for the Pt electrode, such as shown in Fig. 9(b), together with an expected potential profile in Fig. 9(a). The following equation is derived according to Koper and Sluyters:[36,37]

$$I = jA = (U - E)/R_\Omega = I_C + I_F = AC_{DL}(dE/dt) + I_F, \quad (7)$$

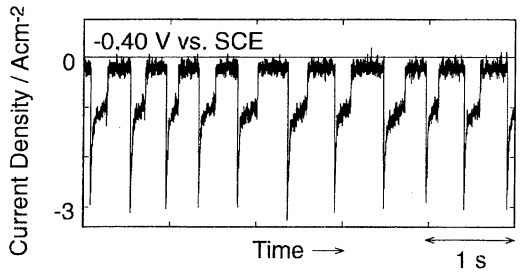

Fig. 6. The waveform of oscillation B at −0.40 V vs. SCE for a Pt disc electrode. Electrode: a Pt disc of 1.0 mm in diameter. Electrolyte: 0.7 M H_2O_2+0.3 M H_2SO_4.

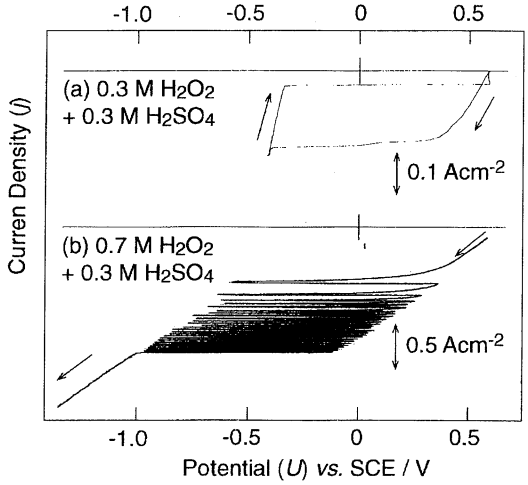

Fig. 7. The j–U curve for a polycrystalline Pt-wire (0.3 mm in diameter and 5 mm long) under a current-controlled condition. The scan rate is (a) 1 mA s^{-1} and (b) 3 mA s^{-1}.

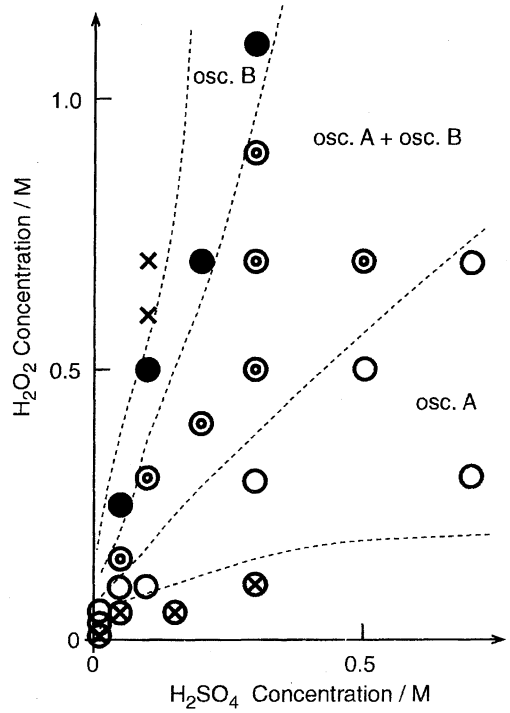

Fig. 8. Phase diagram with respect to the H_2O_2 and H_2SO_4 concentrations. ⊗: no oscillation though the negative resistance appears, ○: only oscillation A appears, ◎: both oscillations A and B appear, ●: only oscillation B appears, and ×: no oscillation nor negative resistance appears.

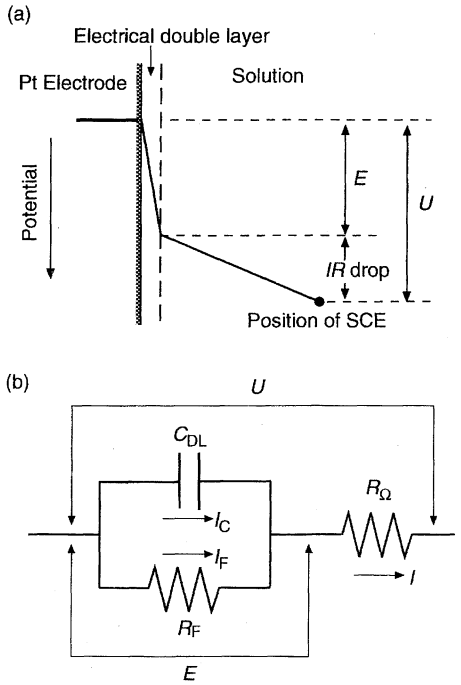

Fig. 9. (a) Schematic potential profile in the region between the electrode surface and the position of SCE, and (b) an equivalent circuit for the electrode including the above region.

where I is the total current, A the electrode area, j the current density, U the (external or applied) electrode potential, E the true electrode potential, $(U-E)$ the ohmic drop between the electrode surface and the position of the reference electrode (SCE), R_Ω the solution resistance in the same place as above, $I_C = AC_{DL}(dE/dt)$ is the charging current, C_{DL} the double-layer capacitance, and I_F the Faradaic current. Equation 7 can be rewritten as

$$dE/dt = (U-E)/AC_{DL}R_\Omega - I_F/AC_{DL}. \tag{8}$$

Now, I_F is given, by taking account of the rates of electrochemical reactions (1), (3), (4), and (5), as follows:

$$I_F = AF\{-k_1 C^s_{H+}(1-\theta_H-\theta_{OH}) + k_{-1}\theta_H - k_3 C^s_{H+}\theta_{OH} + k_4\theta_{OH}^2 - k_5 C^s_{H+}(1-\theta_{OH}-\Theta_H) + k_{-5}\Theta_H\}, \tag{9}$$

where C^s_{H+} is the concentration of H^+ ions at the electrode surface, and θ_{OH}, θ_H, and Θ_H are the surface coverages of Pt–OH, upd-H and on-top H, respectively. The quantities, k_1, k_{-1}, k_3, k_4, k_5, and k_{-5} are the rate constants for the i-th reactions ($i = 1, -1, 3, 4, 5$, and -5), which can be expressed by the Butler–Volmer equations:

$$k_i(E) = k_{i0}\exp[-\alpha_i n_i F(E-E_{i0})/RT], \qquad \text{for } i = 1, 3, \text{ and } 5 \tag{10}$$

$$k_i(E) = k_{i0}\exp[(1-\alpha_i)n_i F(E-E_{i0})/RT], \qquad \text{for } i = -1, 4, \text{ and } -5 \tag{11}$$

where k_{i0} is the rate constant at $E = E_{i0}$, E_{i0} the equilibrium redox potential for the i-th reaction, α_i the transfer coefficient, n_i the number of transferred electrons, F the Faraday constant, R the gas constant, and T the absolute temperature. We can assume for simplicity that $\alpha = 1/2$ for all reactions. Because reactions 1 and -1 (and 5 and -5) are reverse reactions to each other, we obtain $E_{10} = E_{-10}$ and $E_{50} = E_{-50}$.

In oscillating reactions, j, E, C^s_{H+}, C^s_{HO} (the concentration of H_2O_2 at the surface), θ_{OH}, θ_H, and Θ_H are taken as time-dependent variables. The time dependence of C^s_{HO} is expressed as follows:

$$(\delta_{HO}/2)dC^s_{HO}/dt = (D_{HO}/\delta_{HO})(C^b_{HO}-C^s_{HO}) - k_2 C^s_{HO}(1-\theta_H-\theta_{OH})^2, \tag{12}$$

where D_{HO} is the diffusion coefficient for H_2O_2, δ_{HO} the thickness of the diffusion layer for H_2O_2, and C^b_{HO} the concentration of H_2O_2 in the solution bulk. The first term on the right-hand side represents the increase in C^s_{HO} by diffusion, while the second term represents the decrease in C^s_{HO} by reaction (2). The introduction of $(1-\theta_H-\theta_{OH})$ in the second term expresses that reaction (2) proceeds only on a part of naked Pt surface, as mentioned before. [Formally, an expression of $(1-\theta_H-\theta_{OH}-\Theta_H)$ has to be used instead of $(1-\theta_H-\theta_{OH})$ because the formation of on-top H should suppress reaction (2). However, θ_H approaches unity in a potential region where Θ_H takes a meaningful value, and thus the term $(1-\theta_H-\theta_{OH}-\Theta_H)$ becomes negative in such a potential region owing to double counting of occupied sites. Therefore Θ_H was neglected.] In the first term of the right-

hand side, we adopt a model of Nernst's diffusion layer having a constant thickness (δ_{HO}), as is generally done by other workers.[6,36—39] This is mainly due to a limitation of calculation capacity in our calculation program. The term ($\delta_{HO}/2$) on the left-hand side is put to take an average of the H_2O_2 concentration in the diffusion layer.[36,37]

Similarly, the time dependence of C^s_{H+} is expressed, with a small contribution of the drift motion of H^+ being neglected, as follows:

$$(\delta_{H+}/2)\mathrm{d}C^s_{H+}/\mathrm{d}t = (D_{H+}/\delta_{H+})(C^b_{H+} - C^s_{H+}) + \{-k_3 C^s_{H+}\theta_{OH} - k_1 C^s_{H+}(1-\theta_H-\theta_{OH}) + k_{-1}\theta_H - k_5 C^s_{H+}(1-\theta_{OH}-\Theta_H) + k_{-5}\Theta_H\}, \quad (13)$$

where D_{H+} is the diffusion coefficient for H^+ ions, δ_{H+} the thickness of the diffusion layer for H^+, and C^b_{H+} the concentration of H^+ in the solution bulk. We also obtain the following rate equations for adsorbed OH, upd-H, and on-top H.

$$N_0\mathrm{d}\theta_{OH}/\mathrm{d}t = k_2 C^s_{HO}(1-\theta_H-\theta_{OH})^2 - k_3 C^s_{H+}\theta_{OH} - k_4\theta_{OH}^2, \quad (14)$$

$$N_0\mathrm{d}\theta_H/\mathrm{d}t = k_1 C^s_{H+}(1-\theta_H-\theta_{OH}) - k_{-1}\theta_H, \quad (15)$$

$$N_0\mathrm{d}\Theta_H/\mathrm{d}t = k_5 C^s_{H+}(1-\theta_{OH}-\Theta_H) - k_{-5}\Theta_H - 2k_6\Theta_H^2, \quad (16)$$

where N_0 represents the total amount of surface Pt sites per unit area under an assumption that it is the same for adsorbed OH, upd-H, and on-top H.

Figure 10 shows results of numerical calculation in which the external (or applied) electrode potential U is scanned at a constant rate. Figure 11 shows results of calculation in which U is kept constant. The parameter values used for calculations are shown in the caption of Fig. 10. The diffusion coefficients for H_2O_2 (D_{HO})[40—42] and H^+ (D_{H+})[43] were taken from reported values. The $E_{10} = E_{-10}$ was estimated from the j–U curve as the center of the two current peaks for upd-H (Fig. 2(a)). The $E_{50} = E_{-50}$ was also estimated from the observed hydrogen-evolution current. There are no reported data for the E_{20} and k_{i0} values. Thus the E_{20} was taken to be near the onset potential of the H_2O_2-reduction current, and the k_{i0}'s were roughly estimated from the rate constants reported for various metal deposition reactions ($M^{z+}+ze^- \rightarrow M$) which ranged from 10^{-1} to 10^{-4} cm s^{-1}.[44]

The calculated j–U curves in Fig. 10 reproduce the essential features of the observed j–U curves in Figs. 2(b) and 2(c), i.e., the appearance of a negative slope in a low H_2O_2 concentration and that of oscillation A in a high H_2O_2 concentration. The calculated j–t curve in Fig. 11 also reproduces the essential features of the observed curves (Figs. 3 and 4). In addition, the calculations have also reproduced the observed results that the oscillation period for oscillation A increases with decreasing electrode potential (Fig. 3) and decreasing H_2O_2 concentration (Fig. 4). This clearly indicates that the aforementioned reaction model (Fig. 5) is essentially valid for oscillation A. On the other hand, the appearance of oscillation B cannot be reproduced by the present calculations, as is seen in Fig. 10(b). It is likely that another unknown factor has to be taken into account to explain oscillation B.

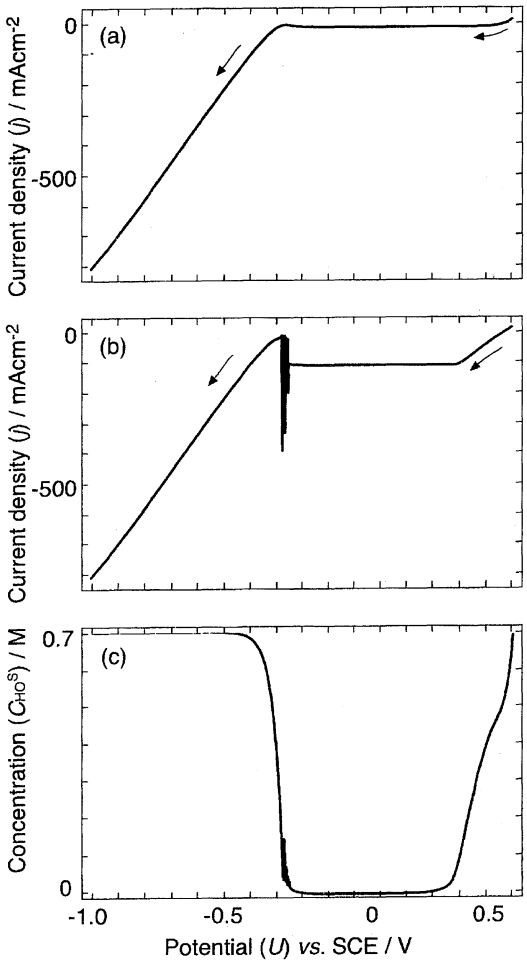

Fig. 10. Calculated j vs. U and C^s_{HO} vs. U curves with U scanned at a rate of 0.02 V s^{-1}. Parameter values used: $C^b_{HO} = 0.1\times10^{-3}$ mol cm^{-3} in (a) and 0.7×10^{-3} mol cm^{-3} in (b) and (c), $\delta_{HO} = 0.01$ cm, $D_{HO} = 1.7\times10^{-5}$ cm^2 s^{-1}, $C^b_{H+} = 0.3\times10^{-3}$ mol cm^{-3}, $\delta_{H+} = 0.004$ cm, $D_{H+} = 9.3\times10^{-5}$ cm^2 s^{-1}, $A = 0.01$ cm^2, $C_{DL} = 2.0\times10^{-5}$ F cm^{-2}, $N_0 = 2.2\times10^{-9}$ mol cm^{-2}, $R_\Omega = 60\Omega$, $T = 300$ K, $\alpha = 0.5$, $n = 1$, $k_{10} = 1.0\times10^{-2}$ cm s^{-1}, $k_{-10} = 1.0\times10^{-5}$ mol cm^{-2} s^{-1}, $k_2 = 4.0\times10^{-2}$ cm s^{-1}, $k_{30} = 1.0\times10^{-5}$ cm s^{-1}, $k_{40} = 1.0\times10^{-8}$ mol cm^{-2} s^{-1}, $k_{50} = 5.0\times10^{-3}$ cm s^{-1}, $k_{-50} = 5.0\times10^{-6}$ mol cm^{-2} s^{-1}, $k_6 = 5.0\times10^{-6}$ mol cm^{-2} s^{-1}, $E_{10} = E_{-10} = -0.19$ V vs. SCE, $E_{30} = 0.8$ V, $E_{40} = 0.4$ V, and $E_{50} = E_{-50} = -0.3$ V. Almost the same results are obtained under an assumption of $C^s_{H+} = C^b_{H+}$.

Figure 12 shows, for reference in later discussion, the calculated θ_H vs. E relation.[25] If the forward and backward processes for reaction (1) are in equilibrium at every potential E, the following equation holds:

$$k_1 C^s_{H+}(1-\theta_H) \cong k_{-1}\theta_H, \quad (17)$$

under an assumption that θ_{OH} is nearly zero in a potential region where upd-H is present. By using Eqs. 10 and 11 for k_1 and k_{-1} together with $\alpha = 1/2$, $n = 1$ and $E_{10} = E_{-10}$, we obtain the following expression for θ_H:

$$\theta_H \cong 1/[1 + (k_{-10}/k_{10}10^{-3})\exp\{(F/RT)(E - E_{10} + \beta p\mathrm{H}^s)\}], \quad (18)$$

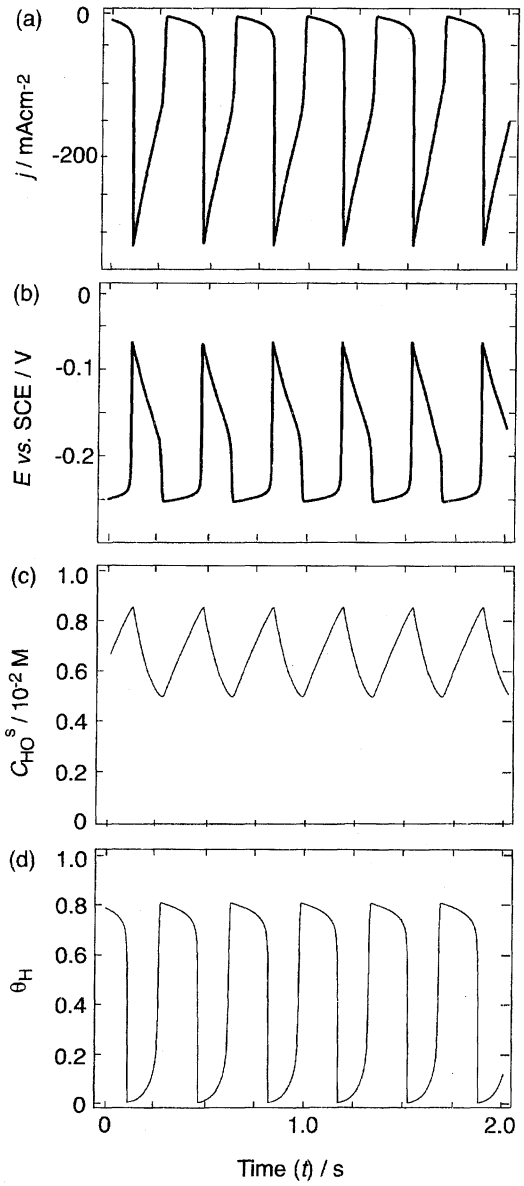

Fig. 11. Calculated j–t, E–t, C^s_{HO}–t, and θ_H–t curves at $U = -0.26$ V vs. SCE. The parameter values used are the same as in Figs. 10(b) and 10(c).

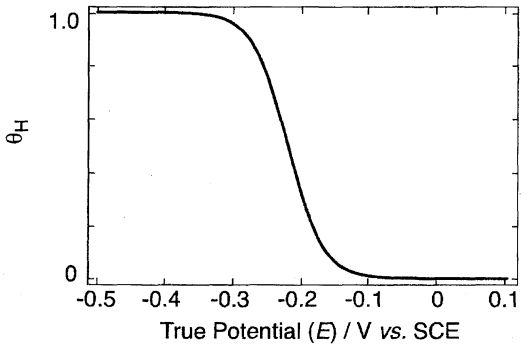

Fig. 12. The surface coverage of upd-H (θ_H) as a function of E, calculated by Eq. 19 with $b = 80\ V^{-1}$, $E_{10} = -0.10$ V vs. SCE, and $pH^s = 0.53$.

where $(k_{-10}/k_{10}10^{-3}) \cong 1$, $\beta = RT(\ln_e 10)/F \cong 0.059$ V at 300 K, and pH^s is the solution pH near the electrode surface. In Fig. 12, not Eq. 18 but the following equation

$$\theta_H \cong 1/[1+\exp\{b(E - E_{10} + \beta pH^s)\}] \quad (19)$$

is plotted with b taken as a parameter by taking account of the presence of the two current peaks for upd-H (Fig. 2(a)) and hence the presence of two kinds of upd-H. We can see that θ_H changes from nearly zero to nearly one in a potential (E) range near $(E_{10} - \beta pH^s) = -0.22$ V.

1.3. Positive Feedback Mechanism in Oscillation A. The oscillation mechanism for oscillation A can be explained on the basis of the above results calculated.[25] Let us first consider the low-current state with low j and high θ_H (see Fig. 11). In this state, little H_2O_2 reduction occurs because of high θ_H, and thus the C^s_{HO} increases with time by diffusion of H_2O_2 from the solution bulk (see the C^s_{HO}–t curve in Fig. 11). Nearly in proportion to the increase in C^s_{HO}, the H_2O_2-reduction current (j) in the low-current state increases with time (the j–t curve in Fig. 11).

Here we have to note that the j in the low-current state flows through a small amount of naked Pt sites not covered with upd-H. Thus the j increases with increasing $(1-\theta_H)$ or decreasing θ_H. The increase in j causes an increase in the ohmic drop in the solution and thus leads to a positive shift in the true electrode potential (E) under a constant applied potential (U) (see Fig. 9(a)). The positive shift in E, in turn, leads to a decrease in θ_H (see Fig. 12). Thus we can see the presence of a positive feedback mechanism. Namely, an increase in j→an increase in the ohmic drop→a positive shift in E→a decrease in θ_H→an increase in j. We have also to note that the θ_H decreases sharply with E when it reaches about 0.7—0.8 (see Fig. 12). Accordingly, as the j increases gradually as mentioned above and hence the θ_H decreases gradually, the θ_H suddenly decreases at a certain time, accompanied by a sudden increase in j (the j–t and θ_H–t curves in Fig. 11).

The inverse process, i.e., a sudden change from the high-current state to the low-current states can be explained similarly. If active H_2O_2 reduction starts with $\theta_H \cong 0$ and it continues, the C^s_{HO} decreases with time due to slow H_2O_2 diffusion (the C^s_{HO}–t curve in Fig. 11), and thus the H_2O_2-reduction current (j) decreases with time (the j–t curve). The decrease in j causes a decrease in the ohmic drop in the solution and hence a negative shift in E, which, in turn, leads to an increase in θ_H and leads to a further decrease in j. Here is also a positive feedback mechanism. Thus, when j reaches a certain critical value and θ_H enters into the region of rapid change with E (Fig. 12), the j suddenly decreases, accompanied by a sharp increase of θ_H.

In conclusion, we can say that the essential mechanism of oscillation A has been clarified. Further studies are now in progress on the clarification of the mechanism of oscillation B.

2. Modulation of Oscillation A by External Perturbations

The oscillatory behavior of oscillation A can be modified by applying external perturbations such as electrode illumination, weak external potential pulses, or coupling with other oscillating systems. Investigations of such modifications by external perturbations are helpful for deeper understanding of oscillation phenomena.

Figure 13 shows a change of the waveform of oscillation A by electrode illumination where the illumination intensity is increased in proportion to time.[26] The oscillation period becomes longer with the increasing illumination intensity, and finally the oscillation stops. Such behavior may partly be explained by a photo-thermal effect, which causes an increase in the temperature and hence an increase in the H_2O_2 concentration near the electrode surface.

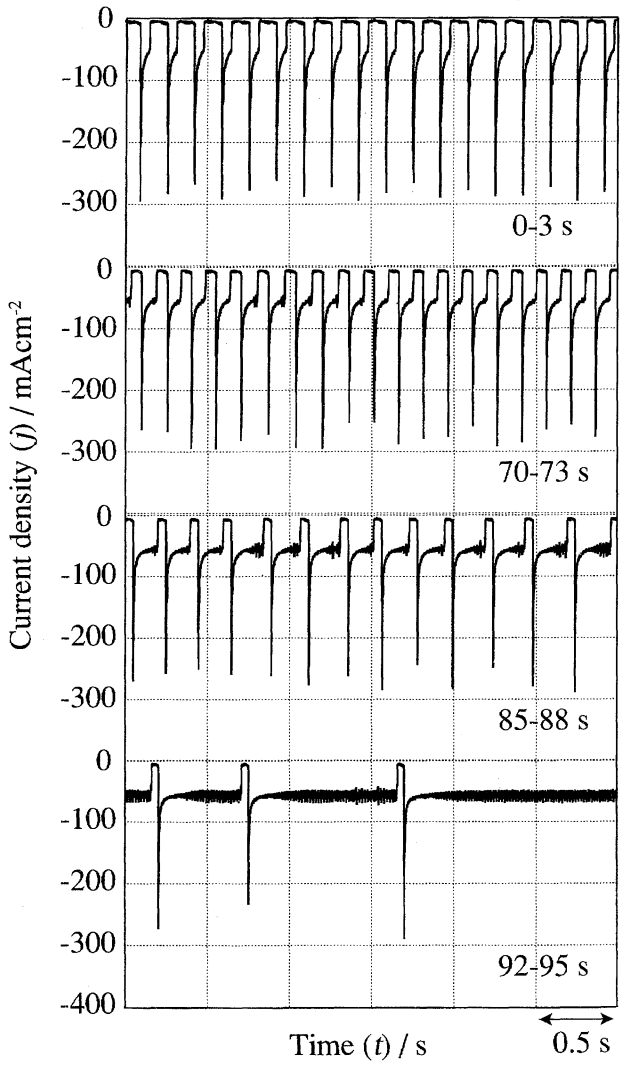

Fig. 13. A change of the waveform of oscillation A by electrode illumination where the illumination intensity is increased in proportion to time at a rate of 1 Ws^{-1} with a 120 V–300 W tungsten-halogen lamp. Electrode potential: −0.26 V vs. Ag/AgCl. Electrolyte: 0.7 M H_2O_2+0.3 M H_2SO_4.

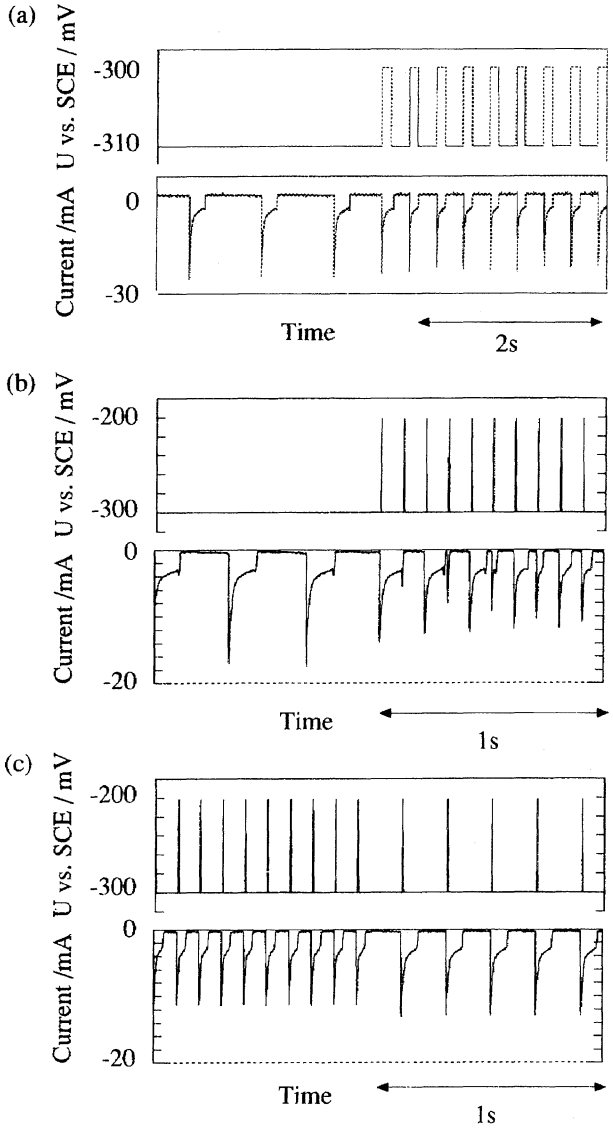

Fig. 14. The synchronization of oscillation A with weak external potential pulses. The upper figures in (a), (b), and (c) indicate external potential pulses added to the electrode potential (U), whereas the lower figures indicate waveforms of oscillation A. The height and width of the external potential pulses are (a) +10 mV, 100 ms and (b) and (c) +100 mV, 1 ms. Electrode: a Pt disc of 1.0 mm in diameter. Electrolyte: 0.7 M H_2O_2+0.3 M H_2SO_4.

Figure 14 shows the effect of applying weak external potential pulses to oscillation A.[27] The oscillation period becomes synchronized with external potential pulses when they are positive in sign and have heights more than about 10 mV. The synchronization can be explained to be due to the removal of upd-H in the low-current state by the positive potential pulse which causes a positive shift in the electrode potential. Such synchronized oscillations enable us to investigate the relation between the duration of the low-current state and the peak current of the high-current state. Detailed analyses supported the oscillation mechanism described in Section 1.[27]

Electrochemical oscillations often show "coupling phe-

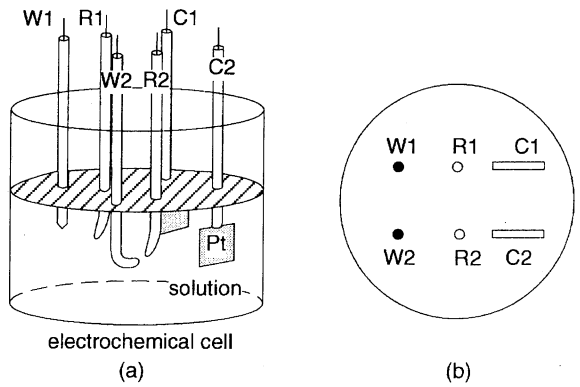

Fig. 15. (a) An electrochemical cell for observing coupling of oscillations, and (b) a top view of the cell. W1, W2: working electrodes, C1, C2: counter electrodes, and R1, R2: reference electrodes.

nomena". Figure 15 shows an experimental setup for observing the coupling. Two electrochemical systems, each composed of a working electrode, a counter electrode, and a reference electrode, are immersed in a common electrolyte solution. When the electrochemical systems are far apart from each other, they show independent oscillations. On the other hand, when they are brought close to each other, the oscillations are coupled, resulting in, e.g., synchronized oscillations. Figure 16 shows an example of coupled oscillations.[23,24] Interestingly, when the electrode arrangements of the two electrochemical systems are made inverse to each other, as shown in Fig. 17(a), contrary to Fig. 15(b), anti-phase synchronization is observed, as shown in Fig. 17(b).

Our detailed studies on the mechanism of synchronization have revealed that it is not caused by mass transport for reactants and/or products but by electrical interaction through the ohmic drops in electrolyte solution(s).[23,24] We can say that the current oscillation in an electrochemical system causes, through the oscillation of the ohmic drop in the solution, an

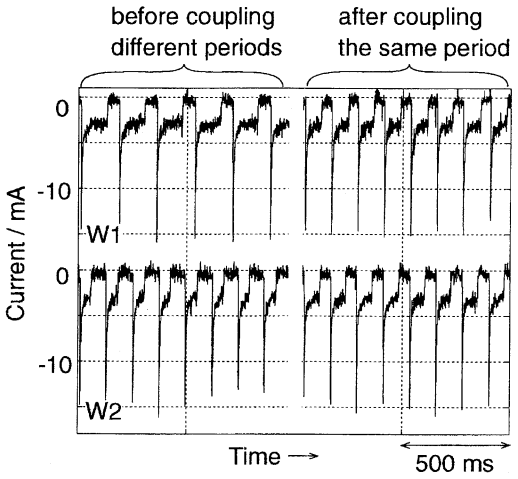

Fig. 16. Currents vs. time for two oscillations before and after coupling. W1 is kept at −0.305 V vs. SCE and W2 at −0.295 V, both being a Pt disc electrode. Electrolyte: 0.7 M H_2O_2+0.3 M H_2SO_4.

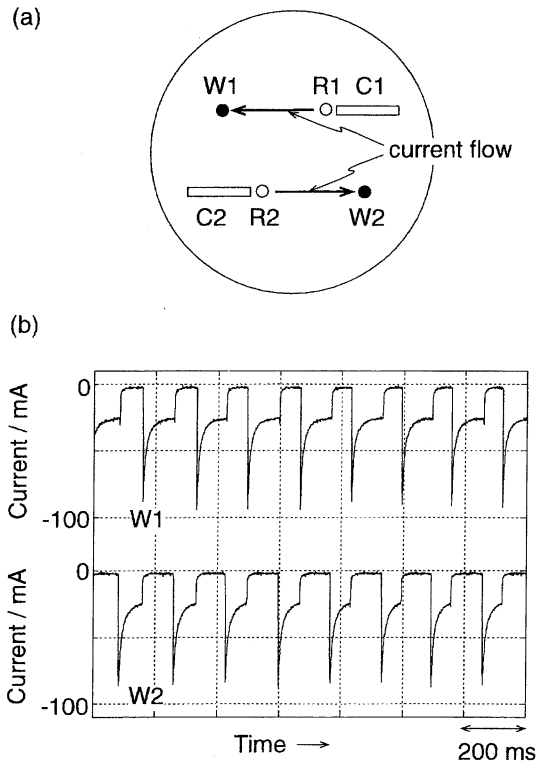

Fig. 17. (a) Electrode arrangement for two electrochemical systems, and (b) anti-phase synchronization observed for the electrode arrangement of (a). Arrows in (a) show the main directions of current flows.

oscillation in the true electrode potential for a neighboring electrochemical oscillation system, which leads to the synchronization of the oscillations. The essential mechanism seems to be the same as the case of applying weak external potential pulses to an oscillatory system described above (Fig. 14).

The oscillatory coupling plays an important role in various aspects of oscillations. For example, even oscillations for one-working-electrode systems such as shown in Fig. 1 are often governed by coupling phenomena, because oscillations at various parts of the electrode surface can couple with each other. Some complex waveforms such as mixed-mode oscillations can be explained in terms of oscillation coupling.

3. Modulation of Oscillation A by Adsorbed Metal Atoms

As mentioned in the introductory section, chemical reactions in oscillating systems proceed synchronically in an in-phase mode. Therefore it is of much interest to investigate the effect of microscopic structures of the electrode surface on the oscillatory behavior and vice versa.

An interesting example is given by the modulation of the oscillation period of oscillation A on a Pt electrode by adsorption of foreign metal atoms such as Cu, Ag, Au, and Ru to sub-monolayer amounts. Experiments are done in which a Pt disc electrode is first immersed in the electrolyte containing metal ions and then the electrode potential is shifted from the rest potential (ca. +0.55 V vs. SCE) to a potential where

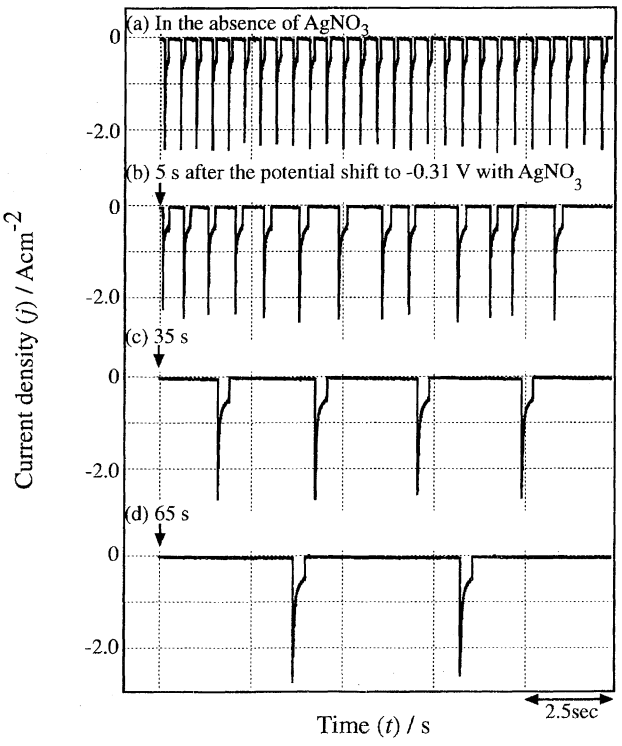

Fig. 18. Time courses of oscillation A at −0.31 V vs. SCE in case where 1.6×10^{-6} M $AgNO_3$ is added to 0.7 M H_2O_2+ 0.3 M H_2SO_4. The time in the figure is scaled with the time of the potential shift taken to be zero.

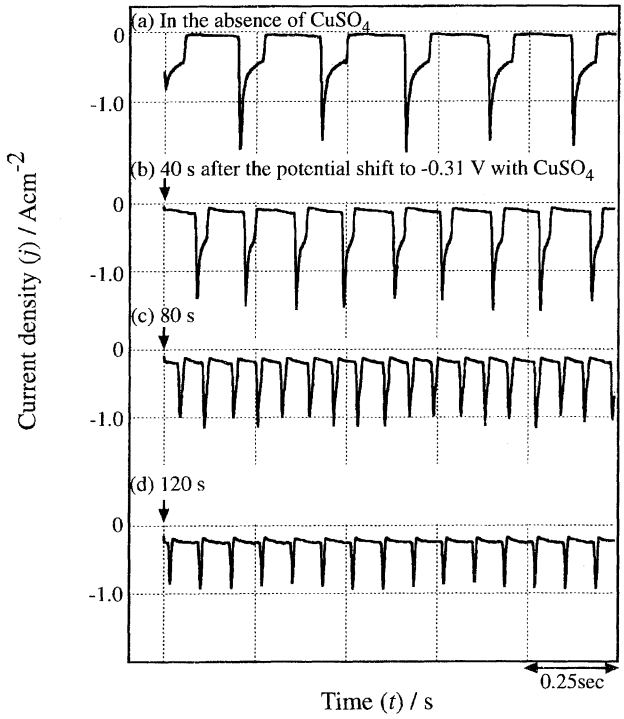

Fig. 19. Time courses of oscillation A at −0.31 V vs. SCE in case where 1.6×10^{-6} M $CuSO_4$ is added to 0.7 M H_2O_2+0.3 M H_2SO_4.

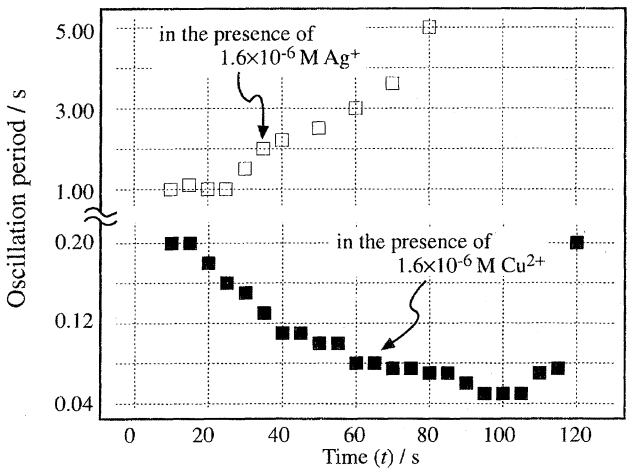

Fig. 20. The oscillation period plotted as a function of time in the presence of Ag^+ and Cu^{2+} ions in the solution.

oscillation A appears. Figure 18 shows a result when a small amount of Ag^+ ions is added to the electrolyte.[28] Oscillation A is stable in the absence of Ag^+ ions without any changes in the waveform and period for more than 1 h (Fig. 18(a)). In the presence of Ag^+, however, the oscillation period becomes longer with time (Figs. 18(b), 18(c), and 18(d)) and finally the oscillation stops. Figure 19 shows a result of a similar experiment in the presence of Cu^{2+} ions. Contrary to the case of Ag^+, the oscillation period becomes shorter with time. Similar results to Fig. 19 are obtained with $AuCl_4^-$ and Ru^{2+}. Figure 20 plots the oscillation period as a function of time in order to show the difference between Ag^+ and Cu^{2+} clearly.

Why does such a difference between Ag^+ and Cu^{2+} arise? It is first to be noted that the metal ions are electrochemically reduced and the corresponding metals are deposited on Pt during the oscillation because the potential at which oscillation A is observed (−0.31 V) is more negative than the redox potentials for the metal deposition.[45,46] In fact, the deposition of Au was confirmed by X-ray photoelectron spectroscopic (XPS) analysis after the oscillation experiments. The deposition of metals was also confirmed by decreases in the heights of the cathodic current peaks for upd-H. Rough estimations of the amount of metal (Au) deposited by the XPS and electrochemical measurements have shown that it is about 0.3 in the surface coverage (θ) for the electrodes just after oscillation A stopped.

Now the above-mentioned difference can be explained as follows: The oscillation patterns in Figs. 18 and 19 show that the change of the oscillation period is mainly caused by the change in the duration time of the low-current state (t_{low}). As mentioned in Section 1.3, the H_2O_2 reduction in the low-current state is almost completely suppressed by a nearly full coverage of upd-H. However, a small H_2O_2-reduction current flows through a small amount of naked Pt sites still remaining uncovered with upd-H, and the current density (j) increases slightly with time between two adjacent current pulses (see Figs. 18 and 19) due to an increase in the surface H_2O_2 concentration by diffusion. A sudden increase in j (or the transition from the low-current state to the high-current state) occurs when the j in the low-current state reaches a critical value (j_c). That is, the t_{low} is determined by j_c. Thus,

if the deposition of a metal, e.g., Ag, on Pt makes the j lower, the t_{low} becomes longer.

It is reported[47] that the H_2O_2 reduction on Ag proceeds via brigde-type adsorption of H_2O_2 on two adjacent Ag atoms, whereas that on Au proceeds via end-on-type adsorption of H_2O_2 on an Au atom. Thus, if Ag is deposited monoatomically in a dispersed form, not forming any aggregates nor islands, no brigde-type adsorption of H_2O_2 is possible and hence the H_2O_2 reduction on the deposited Ag does not occur. This implies that the deposition of Ag atoms leads to a decrease in j in the low-current state and hence to an increase in the t_{low}, in agreement with the experiment. On the other hand, for the deposition of Au, the H_2O_2 reduction occurs even on monoatomically dispersed ad-atoms because the end-on-type adsorption is possible for such adsorption. Thus, the deposition of Au leads to an increase in j in the low-current state (because the H_2O_2-reduction on Au occurs continuously with time though little H_2O_2 reduction occurs on Pt in the low-current state) and hence a decrease in the t_{low}, again in agreement with the experiment. The above arguments are in harmony with the experimental results that the observed current (j) in the low-current state for the deposition of Cu increases with time from 0 to 120 s (Fig. 19), whereas that for the deposition of Ag increases little with time from 0 to 65 s (Fig. 18).

The metal deposition during oscillations may be an interesting system to investigate whether the oscillations can have the power to control the spatial distribution of the deposited metal atoms or not. This subject is now under investigation.

4. Appearance of New-Type Oscillations by Adsorbed Halogen Atoms

4.1. Fundamental Behavior of New-Type Oscillations. It is known that halide ions such as Cl^-, Br^-, and I^- are adsorbed electrochemically on Pt in positive potentials.[48—51] Oscillations A and B, especially oscillation B, are strongly affected by adsorption of halide ions. Moreover, new-type oscillations appear when small amounts of halide ions are added to acidic H_2O_2 solutions.[29,30]

Figure 21 shows a change of the j–U curve for a polycrystalline Pt-disc electrode with increasing concentration of Cl^- added to the solution, measured under current-controlled conditions. The potential oscillation in Fig. 21(a), in which no KCl is added to the solution, is assigned to oscillation B as mentioned before (Fig. 7(b)). When a small amount (2.0×10^{-4} M) of Cl^- is added, a new oscillation, named oscillation C, appears in a range of $|j|$ (the absolute value of j) lower than that for the appearance of oscillation B (Fig. 21(b)). Oscillation C is clearly distinguished from oscillation B by the potential of the low-potential state (U_{LP}) for the potential oscillation. Namely, the U_{LP} for oscillation C is more positive than ca. 0.0 V vs. SCE, whereas that for oscillation B extends to −0.45 V or more negative potentials where hydrogen evolution occurs. The amplitude of oscillation C increases with increasing $|j|$, differently from the case of oscillation B.

Oscillation C starts to appear at the Cl^- concentration

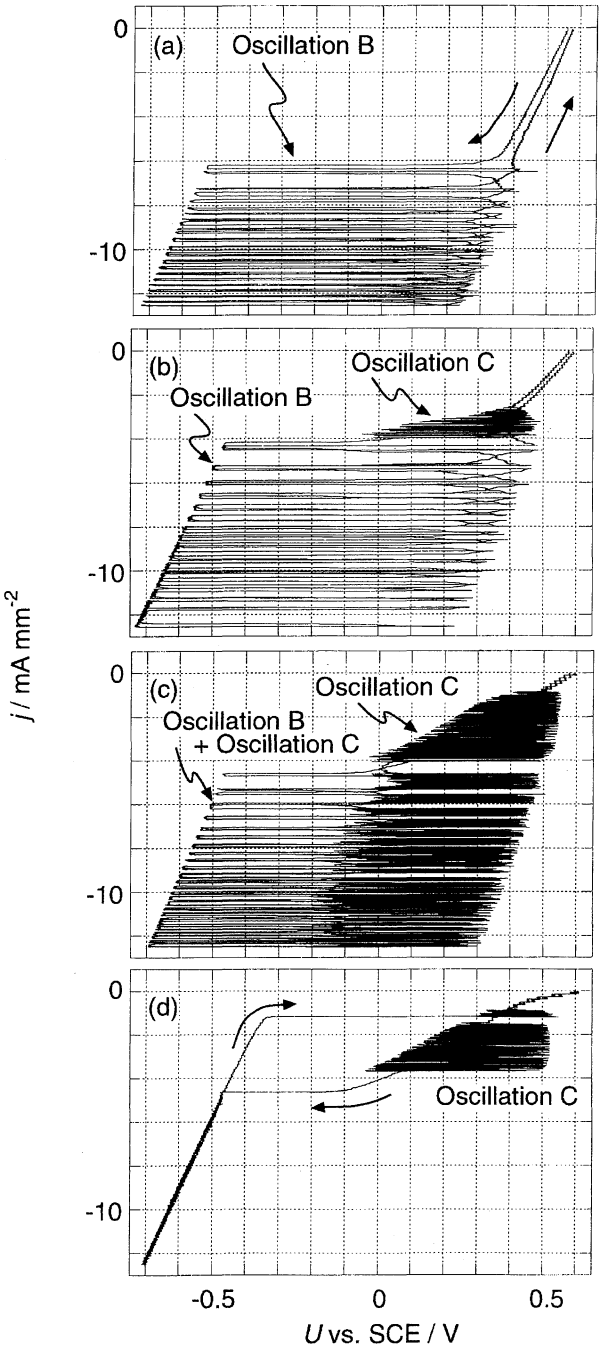

Fig. 21. The j–U curve for a polycrystalline Pt-disc electrode in 0.3 M H_2SO_4+0.7 M H_2O_2+x M KCl where x is (a) 0 M, (b) 2.0×10^{-4} M, (c) 1.0×10^{-3} M, and (d) 3.0×10^{-2} M, measured under a current-controlled condition. The scan rate is 0.25 mA mm^{-2} s^{-1}.

(C_{Cl^-}) of about 5.0×10^{-6} M for a solution of 0.7 M H_2O_2+ 0.3 M H_2SO_4. It becomes more pronounced with increasing C_{Cl^-} and most pronouced at around $C_{Cl^-} = 5.0\times10^{-3}$ M, and then becomes less pronounced, finally disappearing at around 3.0×10^{-2} M. Oscillation B also disappears at high C_{Cl^-} (see Fig. 21(d)). In cases where oscillation C is pronounced, it overlaps oscillation B and thus oscillation B becomes a mixed-mode-type oscillation as seen in Fig. 21(c) (also see Fig. 23(b)). Oscillation C becomes more pronounced with

increasing H_2O_2 concentration at a constant C_{Cl^-}.

Though oscillation C as the potential oscillation is observed in a wide range of C_{Cl^-} as mentioned above, oscillation C as the current oscillation under potential-controlled conditions is observed only temporarily in high H_2O_2 concentrations. Figure 22 shows *j–U* curves in the presence of Cl^- under potential-controlled conditions. Oscillation C as the current oscillation in Fig. 22(b) is not stable at a constant potential, stopping in 5 to 40 s.

Figure 23 shows the waveforms in 0.3 M H_2SO_4+0.7 M H_2O_2+2.0×10^{-4} M KCl at constant current densities of $|j|$ = (a) 3.2 and (b) 5.1 mA mm^{-2}, which are, in Fig. 21(b), in a region of oscillations C and B, respectively. The oscillation period of oscillation C in (a) is about 8 ms, which is much shorter than that for oscillation B in (b), about 4 s. The waveform is also different for oscillations C and B, supporting the assertion that oscillation C is certainly of a new type. Oscillation B in (b) is overlapped with oscillation C in the high-potential state.

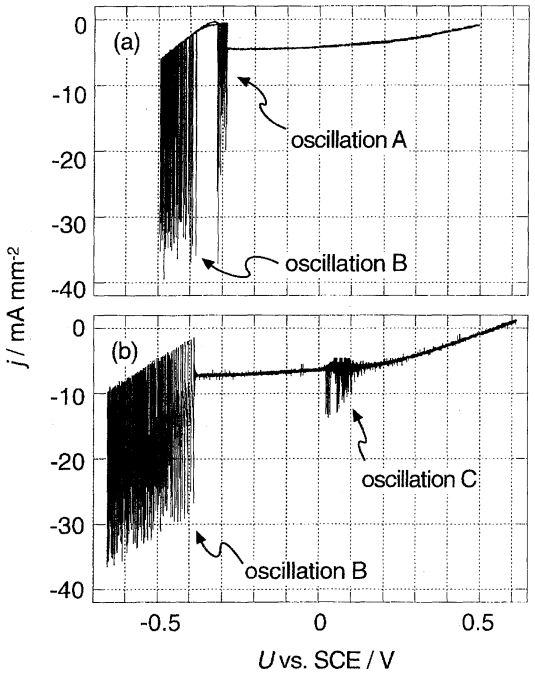

Fig. 22. The *j–U* curves in (a) 0.3 M H_2SO_4+0.7 M H_2O_2+1.0×10^{-3} M KCl and (b) 0.3 M H_2SO_4+1.2 M H_2O_2+1.0×10^{-3} M KCl, measured under a potential-controlled condition. The scan rate is 0.01 V s^{-1}.

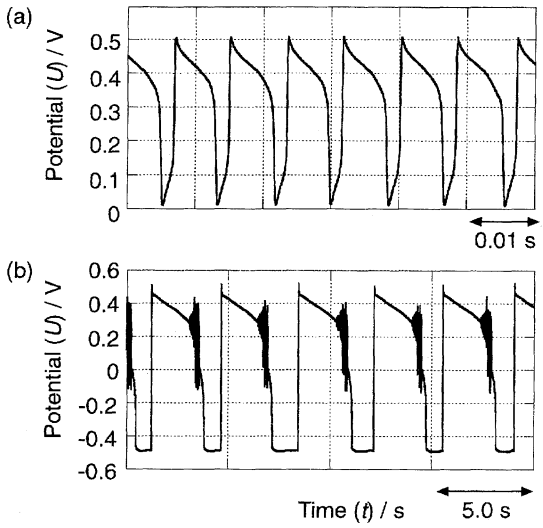

Fig. 23. The waveforms of potential oscillations in 0.3 M H_2SO_4+0.7 M H_2O_2+2.0×10^{-4} M KCl at $|j|$ = (a) 3.2 and (b) 5.1 mA mm^{-2}.

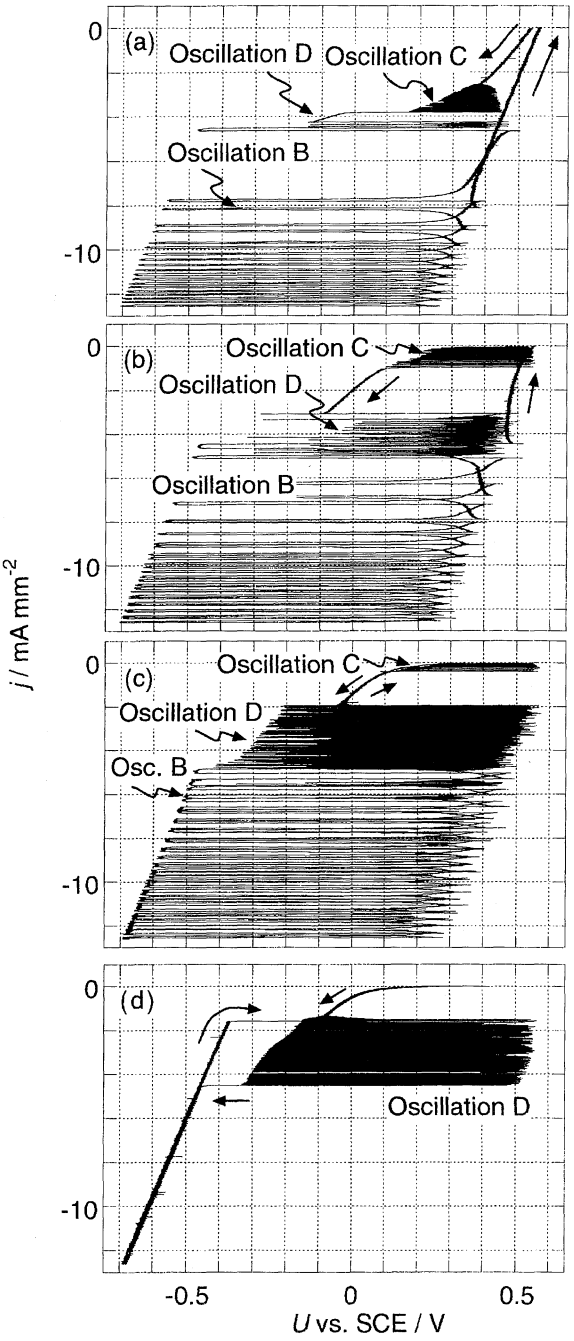

Fig. 24. The *j–U* curves in 0.3 M H_2SO_4+0.7 M H_2O_2+*x* M KBr where *x* is (a) 1.0×10^{-6} M, (b) 1.0×10^{-5} M, (c) 1.0×10^{-4} M, and (d) 3.0×10^{-3} M, measured under a current-controlled condition. The scan rate is 0.25 mA mm^{-2} s^{-1}.

Figure 24 shows j–U curves when Br^- is added to the solution, measured under current-controlled conditions. Another new oscillation, named oscillation D, appears in addition to oscillations B and C. Oscillations B, C, and D can be distinguished by the difference in the U_{LP} as mentioned before. Namely, the U_{LP} for oscillation D is about -0.3 to -0.1 V, which is in between the U_{LP} values for oscillations B and C. At a low Br^- concentration (C_{Br^-}) of 1.0×10^{-6} M, only oscillation C appears. As the C_{Br^-} increases, the region of $|j|$ for oscillation C becomes narrower and moves to the low $|j|$, and finally oscillation C disappears. Oscillation D becomes more pronounced with increasing C_{Br^-} but disappears in too high C_{Br^-}. Oscillation B also disappears in high C_{Br^-}. Interestingly, oscillation D in the presence of Br^- is clearly observed as the current oscillation under potential-controlled conditions, as shown in Fig. 25, contrary to the case of oscillation C in the presence of Cl^- or Br^-.

Figure 26 shows the waveforms of the potential oscillations in the presence of 1.0×10^{-4} M KBr at $|j|$ = (a) 2.5, (b) 3.8, (c) 5.1, and (d) 6.4 mA mm^{-2}. From the current densities and Fig. 24(c), the oscillations in (a), (b), (c), and (d) in Fig. 26 can be assigned to oscillation D (slightly mixed with oscillation C), oscillation D, oscillation B mixed with oscillations C and D, and oscillation B (slightly mixed with oscillation C), respectively. The oscillation period of oscillation D is about 50 ms. Figure 27 shows the waveforms of the current oscillations in the presence of 1.0×10^{-4} M KBr (cf. Fig. 25(b)) at (a) $U = -0.25$ and (b) -0.30 V vs. SCE. The oscillation pattern and period are quite different from each other, indicating that the oscillation in (a) should be assigned to oscillation D whereas that in (b) should be assigned to oscillations A. Oscillation D is also observed when a small amount of I^- is added to the solution.

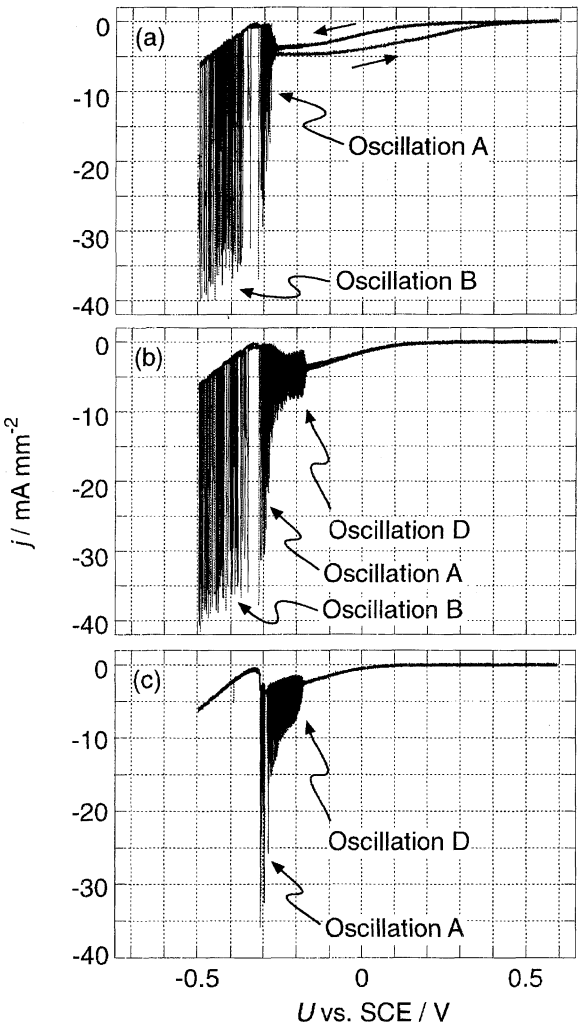

Fig. 25. The j–U curves in 0.3 M H_2SO_4+0.7 M H_2O_2+x M KBr where x is (a) 1.0×10^{-5} M, (b) 1.0×10^{-4} M, and (c) 3.0×10^{-3} M, measured under a potential-controlled condition. The scan rate is 0.01 V s^{-1}.

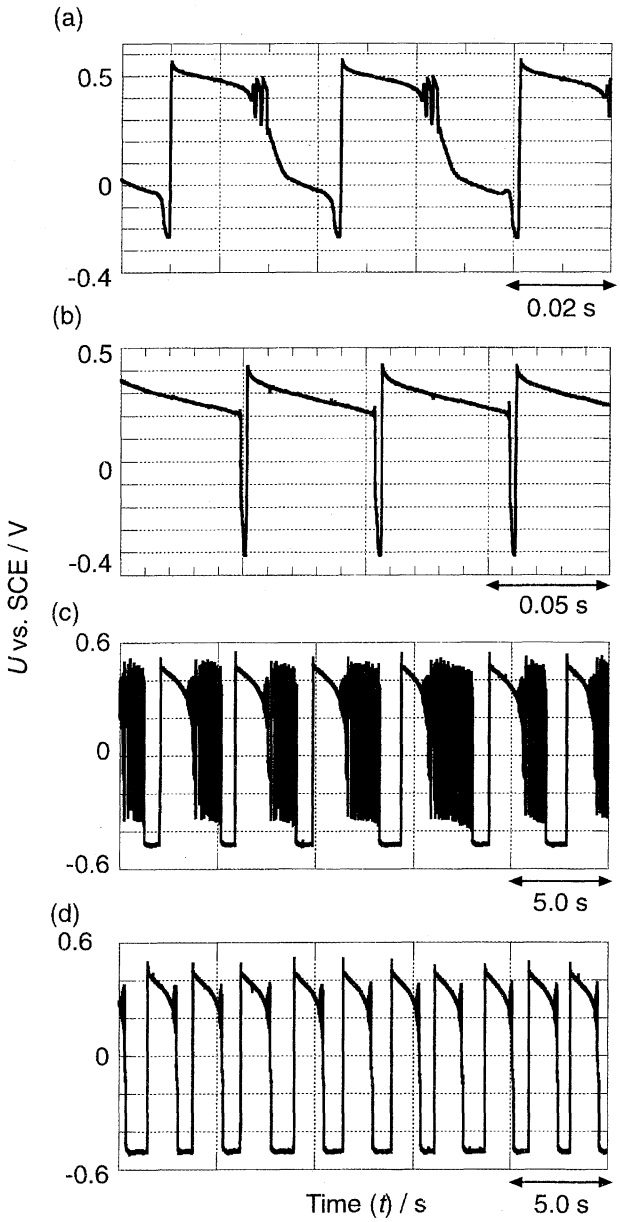

Fig. 26. The waveforms of potential oscillations in 0.3 M H_2SO_4+0.7 M H_2O_2+1.0×10^{-4} M KBr at $|j|$ = (a) 2.5, (b) 3.8, (c) 5.1, and (d) 6.4 mA mm^{-2}.

4.2. Autocatalytic Mechanism. Oscillations C and D are observed only in the presence of halide ions in the

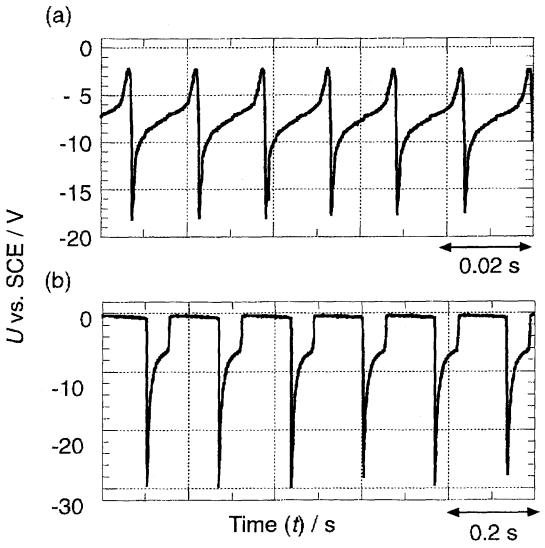

Fig. 27. The waveforms of current oscillations in 0.3 M H_2SO_4+0.7 M H_2O_2+1.0×10^{-4} M KBr at U = (a) −0.25 and (b) −0.30 V vs. SCE.

solution and therefore the mechanism for their appearance should be explained by taking into account the adsorption of halide ions

$$Pt + X^- \underset{k_{-7}}{\overset{k_7}{\rightleftarrows}} Pt\text{–}X + e^- \tag{20}$$

in addition to the reactions described in Section 1.1. Thus we can write the following differential equations, similarly to Section 1.2:

$$(\delta_{HO}/2)dC^s_{HO}/dt = (D_{HO}/\delta_{HO})(C^b_{HO} - C^s_{HO}) - k_2 C^s_{HO}(1 - \theta_H - \theta_{OH} - \theta_X)^2, \tag{21}$$

$$dE/dt = (U - E)/AC_{DL}R_\Omega - I_F/AC_{DL}, \tag{8}$$

$$\begin{aligned} I_F = AF\{&-k_1 C^s_{H+}(1 - \theta_H - \theta_{OH} - \theta_X) \\ &+k_{-1}\theta_H - k_3 C^s_{H+}\theta_{OH} + k_4 \theta_{OH}{}^2 \\ &-k_5 C^s_{H+}(1 - \theta_{OH} - \theta_X - \Theta_H) + k_{-5}\Theta_H \\ &+k_7 C^s_X(1 - \theta_H - \theta_{OH} - \theta_X) - k_{-7}\theta_X\}, \end{aligned} \tag{22}$$

$$N_0 d\theta_{OH}/dt = k_2 C^s_{HO}(1 - \theta_H - \theta_{OH} - \theta_X)^2 - k_3 C^s_{H+}\theta_{OH} - k_4 \theta_{OH}{}^2, \tag{23}$$

$$N_0 d\theta_H/dt = k_1 C^s_{H+}(1 - \theta_H - \theta_{OH} - \theta_X) - k_{-1}\theta_H, \tag{24}$$

$$N_0 d\Theta_H/dt = k_5 C^s_{H+}(1 - \theta_{OH} - \theta_X - \Theta_H) - k_{-5}\Theta_H - 2k_6 \Theta_H{}^2, \tag{25}$$

$$N_0 d\theta_X/dt = k_7 C^s_X(1 - \theta_H - \theta_{OH} - \theta_X) - k_{-7}\theta_X, \tag{26}$$

where θ_X is the surface coverage of X. Equation 8 is applied to results for potential-controlled conditions. Under galvanostatic conditions, the term $(U-E)/AC_dR_\Omega$ in this equation is replaced by (I/AC_d), where I is the total current.

Mathematical simulation with the above equations can, however, not reproduce oscillations C and D even though a wide range of parameter values, which reproduce steady-state current-potential curves such as those shown in Fig. 2(b) as well as the adsorption behavior of halogen atoms reported,[48–51] is tested. The appearance of oscillations C and D can be explained by taking into account a catalytic effect of adsorbed X and an autocatalytic effect of adsorbed OH on the H_2O_2 reduction, by the following equation:

$$k_2 = k_{20} + \gamma\theta_X\theta_{OH}, \tag{27}$$

where k_{20} is the normal rate constant for reaction (2) and γ is a proportional constant. The concept of the above catalytic and autocatalytic effects is supported experimentally by various observations that, for example, the potential-independent H_2O_2-reduction current for single-crystal Pt(111) electrodes is increased by the addition of Br^- to the solution (unpublished results).

Figure 28 shows j–U curves calculated by using Eq. 27 for k_2. The essential feature of oscillation C is reproduced both under current- and potential-controlled conditions, together with that of oscillation A under potential-controlled conditions. Figure 29 shows calculated E–t, θ_X–t, θ_{OH}–t, and C^s_{HO}–t curves at a constant current. Again, the essen-

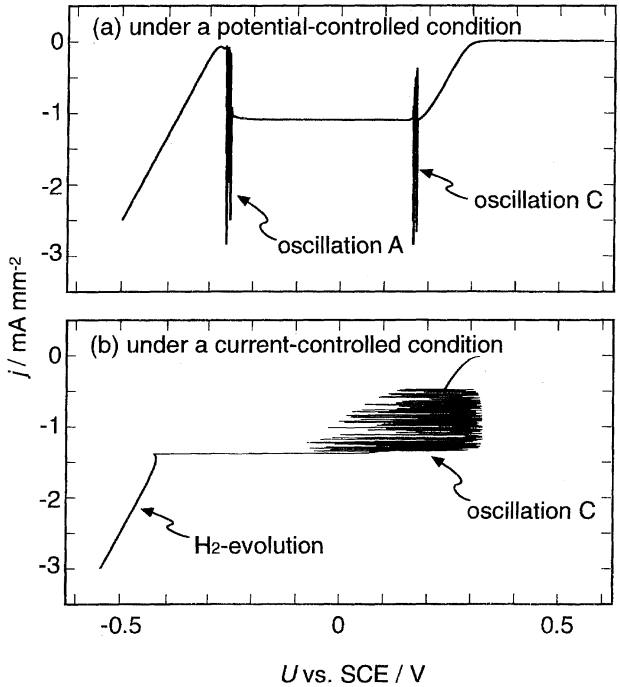

Fig. 28. Calculated j–U curves under (a) potential- and (b) current-controlled conditions, with k_2 expressed as $k_2 = k_{20}+\gamma\theta_X\theta_{OH}$. The scan rate is 0.01 V s^{-1} for (a) and 0.1 mA s^{-1} for (b). The parameter values used: $C^s_{X-} = C^b_{X-} = 1.0\times10^{-5}$ mol cm^{-3}, $C^s_{H+} = C^b_{H+} = 0.3\times10^{-3}$ mol cm^{-3}, $k_{20} = 4.0\times10^{-2}$ cm s^{-1}, $\gamma = 10$ cm s^{-1} for (a) and 1.0 cm s^{-1} for (b), $k_{70} = 1.0\times10^{-4}$ cm s^{-1}, $k_{-70} = 1.0\times10^{-7}$ mol cm^{-2} s^{-1}, and $E_{70} = E_{-70} = 0.1$ V. The other parameter values are the same as those indicated in the caption of Fig. 10.

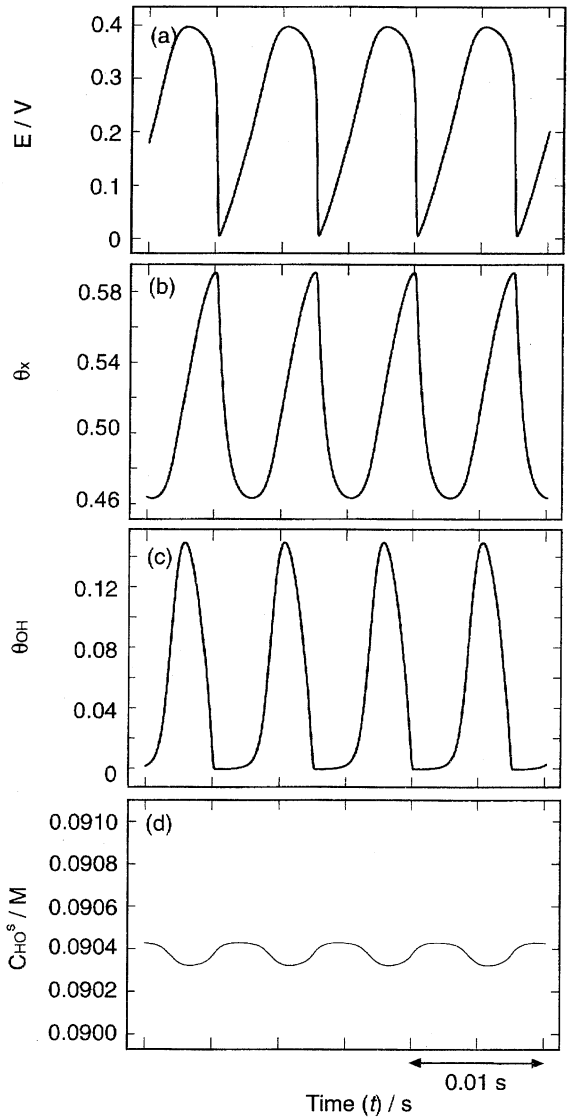

Fig. 29. Calculated E–t, θ_X–t, θ_{OH}–t, and C^s_{HO}–t curves for an oscillation under a galvanostatic condition ($I = -2.0$ mA). The parameter values used are the same as in Fig. 28.

tial feature of the potential oscillation for oscillation C is reproduced.

For comparison, we have also tried to calculate by use of other expressions for k_2 such as

$$k_2 = k_{20} + \gamma' \theta_{OH}, \tag{28}$$

and

$$k_2 = k_{20} + \gamma'' \theta_X. \tag{29}$$

The calculation with Eq. 28 showed the appearance of oscillation C both under current- and potential-controlled conditions, similar to the case of Eq. 27. In this case, however, the calculation showed the appearance of oscillation C even without any adsorption of halogen atoms (reaction (20)), in disagreement with the experiment. The calculation with Eq. 29 reproduced the appearance of oscillation C only under a potential-controlled condition, also in disagreement with the experiment. Further details are now under investigation.

The mathematical simulation described above clearly indicates that oscillation C is quite different in type from oscillation A. Oscillation A is caused by the formation of upd-H, whereas oscillation C is caused by the adsorption of halogen atoms and OH. Instability for oscillation C can arise from the following mechanism. Adsorbed halogen and OH accelerate the dissociative adsorption of H_2O_2 and hence increase the current density for the H_2O_2 reduction, which, in turn, leads to a very low concentration of H_2O_2 at the electrode surface due to its slow diffusion and thus leads to a low current density. The appearance of only oscillation C in Cl^--containing solutions may be attributed to the fact that the Cl^- adsorption is rather weak and occurs only in potentials more positive than 0.0 V vs. SCE.[48—51]

5. New-Type Oscillation Observed at a Single-Crystal Pt(111) Electrode

All the oscillations thus far described are ones observed for polycrystalline Pt electrodes. Their behavior is changed

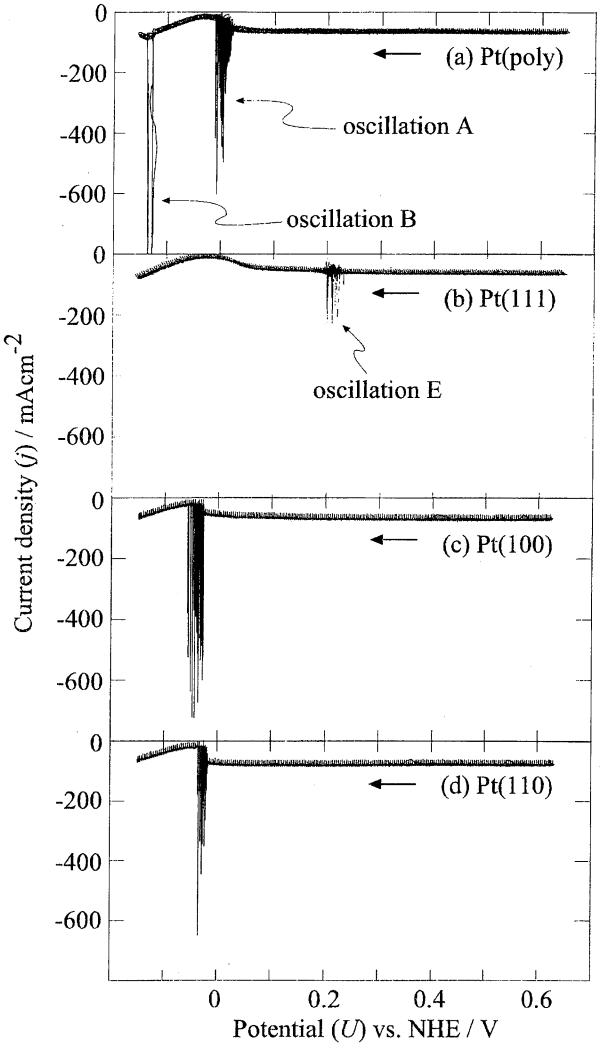

Fig. 30. The j–U curves for Pt(111), (110), and (100) electrodes under a potential-controlled condition, compared with that for polycrystalline Pt. Electrolyte: 0.3 M H_2SO_4+0.7 M H_2O_2. The scan rate: 0.01 V s^{-1}.

by use of atomic-flat single-crystal Pt electrodes. The influence of using low-index single-crystal Pt electrodes on the oscillatory behavior has been studied for the oxidation of hydrogen[10,52] and formic acid.[53,54]

Figure 30 shows the j–U curves for single-crystal Pt(111), (110), and (100) electrodes under potential-controlled conditions, compared with that for a polycrystalline Pt electrode. The single-crystal Pt electrodes were prepared by the method of Clavilier et al.[55] The contact of the well-defined Pt surfaces and the electrolyte was accomplished by making use of a meniscus of the electrolyte. The atomic flatness of the electrodes was confirmed by atomic force microscopy as well as by comparison with the reported characteristic j–U shapes for the hydrogen adsorption and desorption.[56–58]

We can see in Fig. 30 that Pt(110) and (100) electrodes show oscillations similar to "oscillation A" for polycrystalline Pt, whereas Pt(111) shows quite a different oscillation, suggesting that the oscillation for Pt(111) is of a new type. This conclusion is supported by the fact that Pt(111) shows an additional oscillation similar to "oscillation A" when the H_2O_2 concentration is made higher. The new oscillation for Pt(111) can be called "oscillation E". Preliminary experiments show that oscillation E is likely to arise from the autocatalytic effect of adsorbed OH. Further details are now under investigation.

6. Conclusions

As described thus far, the electrochemical reduction of H_2O_2 on Pt shows a variety of oscillations, such as those named oscillation A, B, C, D, and E, depending on experimental conditions. This is a unique feature of this oscillation system, and their comparative studies should be effective for deeper understanding of oscillation phenomena.

Of the oscillations mentioned above, the mechanism of oscillation A has been clarified both experimentally and by mathematical simulation. The mechanism of oscillation C has also been clarified to a considerable extent. The analyses of the oscillations have shown clearly the presence of a positive feedback mechanism and an autocatalytic mechanism, both of which are characteristic of oscillatory phenomena, together with the important roles of adsorbed species such as upd-H and adsorbed halogen.

The oscillatory behavior is largely modified by various external perturbations such as electrode illumination, application of weak external potential pulses, coupling with other oscillatory systems, and adsorption of foreign metal atoms such as Cu, Ag, Au, and Ru to submonolayer amounts. Such modifications are useful to get detailed understanding of oscillatory phenomena.

It is to be noted finally that the above results clearly show an important role of atomic-level structures of the electrode surface in oscillations. Detailed studies along this line may open a new possibility of controlling microscopic structures of the electrode surfaces.

This work was partly supported by a Grant-in-Aid for Scientific Research on Priority Area of "Electrochemistry of Ordered Interfaces" No. 09237105 from the Ministry of Education, Science, Sports and Culture. The authors would like to thank Mr. T. Matsuda, Mr. H. Hommura, Mr. T. Nishimura, Mr. H. Konishi, and Mr. K. Karasumi of Osaka University and Prof. N. Furuya of Yamanashi University for their kind collaborations.

References

1 A. M. Zhabotinski, *Proc. Acad. Sci. USSR*, **157**, 392 (1964).
2 I. R. Epstein and K. Showalter, *J. Phys. Chem.*, **100**, 13132 (1996).
3 J. L. Hudson and T. T. Tsotsis, *Chem. Eng. Sci.*, **49**, 1493 (1994).
4 T. Z. Fahidy and Z. H. Gu, "Modern Aspects of Electrochemistry," ed by R. E. White, J. O'M. Bockris, and R. E. Conway, Plenum, New York (1995), Vol. 27, p. 383.
5 M. T. M. Koper, "Advances in Chemical Physics," ed by I. Prigogine and S. A. Rice, John Wiley & Sons, New York (1996), Vol. 92, p. 161.
6 U. F. Franck and R. FitzHugh, *Z. Elektrochem.*, **65**, 156 (1961).
7 S. Nakabayashi, K. Zama, and K. Uosaki, *J. Electrochem. Soc.*, **143**, 2258 (1996).
8 N. Shinohara, N. Kaneko, and H. Nezu, *Denki Kagaku*, **63**, 419 (1995).
9 T. Yamazaki and T. Kodera, *Electrochim. Acta*, **34**, 969 (1989).
10 K. Krischer, M. Luebke, W. Wolf, M. Eiswirth, and G. Ertl, *Electrochim. Acta*, **40**, 69 (1995).
11 S. Nakabayashi and A. Kira, *J. Phys. Chem.*, **96**, 1021 (1992).
12 H. Okamoto, N. Tanaka, and M. Naito, *Electrochim. Acta*, **39**, 2471 (1994).
13 H. Tributsch, *Ber. Bunsenges. Phys. Chem.*, **79**, 570, 580 (1975).
14 H. Tributsch and J. C. Bennett, *Ber. Bunsenges. Phys. Chem.*, **80**, 321 (1976).
15 S. Cattarin and H. Tributsch, *J. Electrochem. Soc.*, **137**, 3475 (1990).
16 S. Cattarin, H. Tributsch, and U. Stimming, *J. Electrochem. Soc.*, **139**, 1320 (1992).
17 N. Fetner and J. L. Hudson, *J. Phys. Chem.*, **94**, 6506 (1990).
18 M. T. M. Koper, E. A. Meulenkemp, and D. Vanmaekelbergh, *J. Phys. Chem.*, **97**, 7337 (1993).
19 T. G. J. van. Verooij and M. T. M. Koper, *Electrochim. Acta*, **40**, 1689 (1995).
20 G. Flaetgen, K. Krischer, and G. Ertl, *J. Electroanal. Chem.*, **409**, 183 (1996).
21 H. Hommura, Y. Mukouyama, T. Matsuda, S. Yae, and Y. Nakato, *Chem. Lett.*, **1996**, 391.
22 T. Matsuda, H. Hommura, Y. Mukouyama, S. Yae, and Y. Nakato, *J. Electrochem. Soc.*, **144**, 1988 (1997).
23 Y. Mukouyama, H. Hommura, T. Matsuda, S. Yae, and Y. Nakato, *Chem. Lett.*, **1996**, 463.
24 T. Matsuda, Y. Mukouyama, H. Hommura, S. Yae, and Y. Nakato, *J. Electrochem. Soc.*, **144**, 2997 (1997).
25 Y. Mukouyama, H. Hommura, S. Nakanishi, T. Nishimura, H. Konishi, and Y. Nakato, *Bull. Chem. Soc. Jpn.*, **72**, 1247 (1999).
26 Unpublished results.
27 T. Nishimura, Y. Mukouyama, S. Nakanishi, H. Konishi,

and Y. Nakato, *Kagaku-Kogaku Ronbun-shu*, in press (1999).
28 S. Nakanishi, H. Hommura, Y. Mukouyama, T. Matsuda, and Y. Nakato, *Chem. Lett.*, **1998**, 977.
29 Y. Mukouyama, H. Konishi, S. Nakanishi, and Y. Nakato, *Chem. Lett.*, **1998**, 1009.
30 Y. Mukouyama, S. Nakanishi, H. Konishi, and Y. Nakato, *J. Electroanal. Chem.*, **473**, 156 (1999).
31 R. J. Nichols and A. Bewick, *J. Electroanal. Chem.*, **243**, 445 (1988).
32 H. Kita, Y. Gao, S. Ye, and K. Shimazu, *Bull. Chem. Soc. Jpn.*, **66**, 2877 (1993).
33 R. Gerischer and H. Gerischer, *Z. Phys. Chem. N. F.*, **6**, 178 (1956).
34 V. D. Winkelmann, *Z. Elektrochem.*, **60**, 731 (1956).
35 R. Memming, *J. Electrochem. Soc.*, **116**, 785 (1969).
36 M. T. M. Koper and J. H. Sluyters, *J. Electroanal. Chem.*, **303**, 73 (1991).
37 M. T. M. Koper and J. H. Sluyters, *J. Electroanal. Chem.*, **347**, 31 (1993).
38 L. Pohlmann, G. Neher, and H. Tributsch, *J. Phys. Chem.*, **98**, 11007 (1994).
39 M. T. M. Koper and D. M. Vanmaekelbergh, *J. Phys. Chem.*, **99**, 3687 (1995).
40 D. M. H. Kern, *J. Am. Chem. Soc.*, **76**, 4208 (1954).
41 J. J. Lingane and P. J. Lingane, *J. Electroanal. Chem.*, **5**, 411 (1963).
42 V. G. Prabhu, L. R. Zarapkar, and R. G. Dhaneshwar, *Electrochim. Acta*, **26**, 725 (1981).
43 P. W. Atkins, "Physical Chemistry," 4th ed, Oxford University Press, Oxford (1990).
44 N. Tanaka and R. Tamamushi, *Electrochim. Acta*, **9**, 963 (1964).
45 D. M. Kolb, M. Przasnyski, and H. Gerischer, *J. Electroanal. Chem.*, **54**, 25 (1974).
46 "Chemical Handbook (Kagaku Binran)," 4th ed, Basic Part II, The Chemical Society of Japan, Maruzen, Tokyo (1993), p. II-466.
47 K. Jüttner, *Electrochim. Acta*, **29**, 1597 (1984).
48 V. S. Bagotzky, Yu. B. Vasilyev, J. Weber, and J. N. Pirtskhalava, *J. Electroanal. Chem.*, **27**, 31 (1970).
49 G. Horányi, J. Solt, and F. Nagy, *J. Electroanal. Chem.*, **31**, 95 (1971).
50 G. Horányi and E. M. Rizmayer, *J. Electroanal. Chem.*, **83**, 367 (1977).
51 G. Horányi and G. Inzelt, *J. Electroanal. Chem.*, **86**, 215 (1978).
52 M. Eiswirth, M. Luebke, K. Krischer, W. Wolf, J. L. Hudson, and G. Ertl, *Chem. Phys. Lett.*, **192**, 254 (1992).
53 F. Raspel, R. J. Nichols, and D. M. Kolb, *J. Electroanal. Chem.*, **286**, 279 (1990).
54 P. Strasser, M. Luebke, F. Raspel, M. Eiswirth, and G. Ertl, *J. Chem. Phys.*, **107**, 979 (1997).
55 J. Clavilier, R. Faure, G. Guinet, and D. Durand, *J. Electroanal. Chem.*, **107**, 205 (1980).
56 A. Wieckowski, P. Zelenav, and K. Varga, *J. Chim. Phys.*, **88**, 1247 (1991).
57 T. Wagner and P. N. Ross, *J. Electroanal. Chem.*, **250**, 301 (1988).
58 M. Feliu, J. M. Orts, R. Gomez, A. Aldaz, and J. Clavilier, *J. Electroanal. Chem.*, **372**, 265 (1994).

Yoshihiro Nakato was born in Matsusaka, Mie, in 1942. He graduated from Department of Chemistry, Faculty of Engineering Science, Osaka University, in 1965, and received his doctor degree from Osaka University in 1972. He was appointed as a research associate at the above Department in 1969 and then as an associate professor at Laboratory for Chemical Conversion of Solar Energy, Faculty of Engineering Science, Osaka University in 1981. He was promoted to a full professor at Department of Chemistry, Faculty of Engineering Science, Osaka University in 1990. During 1976-1978, he stayed at Laboratory of Prof. H. Gerischer, Fritz-Haber-Institut der Max-Planck-Gesellschaft, Berlin as a visiting researcher. His current research interest includes new-type solar cells, photodecomposition of water, nanometer-scale structuring of metal and semiconductor surfaces, and non-linear chemical phenomena. He received the progress award for young chemists from the Chemical Society of Japan in 1977 and the scientific award from the Japanese Photochemistry Association in 1991.

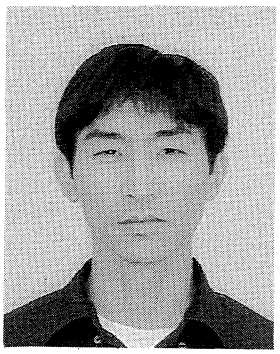

Shuji Nakanishi was born in Osaka in 1973. He graduated from Department of Chemistry, Faculty of Engineering Science, Osaka University, in 1996. He is now a student of Graduate School of Engineering Science, Osaka University. His current interest is directed to the chemistry of atomic-flat metal surfaces and non-linear chemical phenomena.

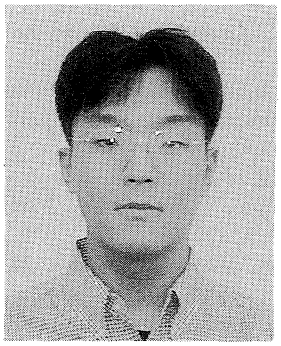

Yoshiharu Mukouyama was born in Shizuoka in 1973. He graduated from Department of Chemistry, Faculty of Engineering Science, Osaka University, in 1995. He is now a student of Graduate School of Engineering Science, Osaka University. His current interest is directed to non-linear phenomena and computational chemistry.